

SOME ASPECTS OF MODELLING OF THE
HIGH TEMPERATURE MECHANICAL BEHAVIOUR OF
NICKEL BASE SUPERALLOYS

R N GHOSH

Computer Applications Division
National Metallurgical Laboratory
Jamshedpur 831 007

ABSTRACT

On the basis of a new physical model based approach a computer package named CRISPEN has been developed jointly by the Cambridge University and the National Physical Laboratory, Teddington. This system allows creep strain prediction for engineering alloys subject to various stress and temperature histories using a set of three coupled differential equations. The first describes the strain rate in terms of stress, temperature and two internal state variables: an internal stress and a damage parameter. The other two describe the rate of evolution of the internal stress and the damage. A major unresolved problem is the detailed form of the equations describing the evolution of the internal state variables. Different classes of material may require an altogether different set of equations. However using the simplest possible approach CRISPEN does predict fairly well the creep behaviour of the class of material exhibiting either linear or exponential strain softening such as the superalloys. A detailed analysis of the creep data of a range of superalloys reveals that under certain conditions both of these mechanisms may occur in parallel.

This report explores how the existing package could be modified to simulate the creep behaviour of materials where both linear and exponential softening mechanisms operate in parallel. The present CRISPEN system assumes the material to be isotropic. The report also examines how the existing formulation could be modified to incorporate full crystallographic anisotropy to simulate the orientation dependence of the creep behaviour of single crystal superalloys.

The mechanisms of deformation in certain other forms of material testing such as stress relaxation, low cycle fatigue or constant strain rate tests are similar as in creep. Therefore CRISPEN type analysis could possibly be extended to describe such tests as well.

An attempt has also been made to describe in this report how this could be implemented. Existing data base on superalloys has been used to demonstrate the potential of this approach.

1. INTRODUCTION

The performance of a high temperature structural material is judged by its ability to withstand the operating stress for a sufficiently long time with minimum accumulation of plastic strain or microstructural damage. Constant stress/load creep test is a convenient method of evaluating this in a laboratory. The results being presented in the form of a strain-time plot for a given stress and temperature. The plastic strain at a given time is expected to be a function of the stress, the temperature, the microstructure and the extent of accumulated structural damage.

An atlas of such plots for a range of stress and temperature forms the basis of the current design practice against creep. The method followed is purely empirical and therefore its accuracy would depend on the availability of test data under conditions very close to those encountered in actual operation. This is often impossible to get because of the unusually long testing time involved. Extrapolation of short term test data may lead to unrealistic predictions particularly when the mechanism of deformation under the actual operating condition is different from the ones encountered during testing.

A design approach based on the actual microstructural changes that take place in the material during service would no doubt be more scientific. In the past several attempts have been made to model the high temperature material behaviour in terms of either the dislocation structure that develops or the structural changes associated with diffusion controlled transformations that may take place during service. Many of these offer excellent quantitative description of the process. However the parameters used to describe these are often difficult to evaluate from simple laboratory tests.

Recent developments of the CRISPEN⁽¹⁻³⁾ system based on a physics based model offers a scope of developing an alternative approach to the current design practice against creep. Using the concept of a two bar model to represent a two phase material it has been shown⁽¹⁾ that the process of creep could be adequately described by the following set of three coupled differential equations:

$$\dot{\epsilon} = \dot{\epsilon}_{SS} \left[\frac{1 - \sigma_1/\sigma}{1 - \sigma_1^*/\sigma} \right] f(\omega) \quad (1)$$

$$\dot{\sigma}_1 = H \dot{\epsilon}_{SS} \left[\frac{\sigma_1^*/\sigma - \sigma_1/\sigma}{(\sigma_1^*/\sigma) (1 - \sigma_1^*/\sigma)} \right] \quad (2)$$

$$\dot{\omega} = k \dot{\epsilon}_{SS} g(\omega) \quad (3)$$

Where the equation 1 describes the strain rate ($\dot{\epsilon}$) as a function of the steady state creep rate ($\dot{\epsilon}_{SS}$), applied stress (σ) and two internal state variables viz internal stress (σ_i) and damage (ω). The subsequent two equations define how σ_i and ω build up during the process of deformation. As σ_i approaches a limiting value of σ_i^* the rate of change of internal stress σ_i would become negligible and $\dot{\epsilon}$ would approach the steady state value of $\dot{\epsilon}_{SS}$ which is often given by the following power law:

$$\dot{\epsilon}_{SS} = \dot{\epsilon}_0 \left[\frac{\sigma}{\sigma_0} \right]^n \quad (4)$$

where σ_0 and $\dot{\epsilon}_0$ are the reference stress and the reference creep rate respectively.

The creep curves of most engineering materials exhibit a prominent tertiary stage where the strain rate continues to accelerate. This may be caused by a variety of damage mechanisms. These have been classified and documented by Ashby and Dyson^(4,5). Present CRISPEN version has the capability of analysing two distinct types of intrinsic softening behaviour of materials viz time softening and strain softening. Materials such as the low alloy steels where the precipitates undergo a time dependent growth during service is expected to follow the time softening model. Dyson and McLean⁽⁶⁾ have shown that in such a situation the exact forms of the functions f and g in equations 1 and 3 are given by:

$$f(\omega) = (1 + \omega)^n \quad (5)$$

$$g(\omega) = a(1 - b\omega)^4 \quad (6)$$

where a and b are constants.

Most nickel base superalloys on the other hand exhibit a strain softening behaviour as a result of continuously increasing mobile dislocation density (or velocity)⁽⁶⁾. Depending on whether the strain acceleration is independent or dependent on the current value of dislocation density two different models have been identified. Linear strain-softening model is based on the assumption that an increment in strain leads to a proportionate increase in either the dislocation density (ρ) or velocity. Thus the functions f and g can be shown to have the following form:

$$f(\omega) = g(\omega) = (1 + \omega) \quad (7)$$

Whereas in the exponential softening model the increment in ρ is proportional to its current magnitude. Consequently the functions of f and g of equations 1 and 3 are given by

$$f(\omega) = g(\omega) = \exp(\omega)$$

(8)

TABLE 1

PARAMETERS DIRECTLY MEASURABLE FROM THE CREEP CURVE

1	Primary creep strain	ϵ_p
2	Primary time constant	t_p (s)
3	Minimum creep rate	$\dot{\epsilon}_{min}$ (s ⁻¹)
4	Tertiary time constant	t_t (s)
5	Failure time	t_f (s)
6	Failure strain	ϵ_f
7	Stress exponent	n
8	Activation energy for creep	Q_1 (kJ/mol)

The model parameters used in equations 1-3 can be determined easily from a set of creep strain-time plots for a specific material. Table 1 gives a list of parameters, directly measurable from a creep curve (Figure 1). The relationship between these measurable characteristics of creep curves and the model parameters used in CRISPEN are given in Table 2 for a case where exponential softening model is operative.

TABLE 2

Relationship between measured characteristics of creep curves and the parameters of the combined models of primary and exponential strain-softening for the case when $t_t > t_p$.

Model Parameter	Measured Characteristics
$\dot{\epsilon}_1 = \dot{\epsilon}_{ss} = \dot{\epsilon}_0 \left[\frac{\sigma}{\sigma_0} \right]^n$	$\dot{\epsilon}_{min}$
σ_1^*/σ	$\left[1 + \frac{\dot{\epsilon}_{min} t_p}{\epsilon_p} \right]^{-1}$
H/σ	$\left[\epsilon_p \left[1 + \frac{\dot{\epsilon}_{min} t_p}{\epsilon_p} \right]^2 \right]^{-1}$
C	$\ln 4.9/2(\dot{\epsilon}_{min} t_t)$

Some of these can however be estimated more precisely by a least square analysis of the relevant portion of the $\dot{\epsilon}$ vs ϵ plots. Such plots also reveal the suitable softening mechanism for a specific material. Figure 2 shows a set of $\dot{\epsilon}$ vs ϵ plots used to identify whether linear or exponential model is applicable for a given material. Integration of the equations 1-3 using the parameters thus obtained provides the creep strain time plot (Figure 3). Following this approach creep behaviour could be predicted for conditions where no data is available by interpolation or extrapolation of the existing parameter data base. This approach has been discussed by Ion et al⁽¹⁾ and Barbosa et al⁽²⁾ in great detail to show how such analysis could provide reasonable predictions even in cases where the stress or the temperature undergo cyclic variation⁽³⁾. The present Crispen package is however applicable to isotropic materials deforming to high creep strains under constant stress by any one of the above softening mechanisms.

Analysis of the creep data on superalloys over a range of stress and temperature reveal that under certain conditions both exponential and linear softening mechanisms operate in parallel. Therefore it is necessary to develop a method of isolating the respective contribution of each to extend the scope of the existing version of Crispen. A section of this report examines how this can be implemented.

Nickel base single crystal superalloys are now extensively used in critical components in modern aero-gas-turbines. $\langle 001 \rangle$ is the most preferred orientation because of its good combination of creep and thermal fatigue behaviour although creep resistance of $\langle 111 \rangle$ can be substantially greater than that of $\langle 001 \rangle$ ⁽⁷⁻⁹⁾. Crispen package can no doubt be used to analyse the creep behaviour of such an alloy of given orientation. However since it is based on tensile formulation it can neither compute the change in orientation of the crystal during creep nor predict the creep behaviour of any alternate orientation. Present report also examines how the existing model could be changed into shear formulation to simulate the orientation dependence of the creep behaviour of single crystal superalloys.

The mechanisms of deformation in certain other forms of material testing such as stress relaxation, low cycle fatigue or constant strain rate tests are similar to those in creep. Therefore in principle the approach used in Crispen could be extended to model such tests as well. In fact to a limited extent the existing package has been used to model the creep behaviour under cyclic loading. The present report examines in detail how the existing system could be reformulated into a universal model capable of simulating all forms of uniaxial mechanical tests at elevated temperature.

2. COMBINED STRAIN SOFTENING MODEL

Figure 4 shows a typical $\dot{\epsilon}/\dot{\epsilon}_1$ vs ϵ plot of a Nickel base superalloy IN738DS under conditions where both linear and exponential strain softening occur in parallel. In such a case the strain rate could be described by the following equation

$$\ln (\dot{\epsilon}/\dot{\epsilon}_1) = \ln (1 + C \epsilon) + k \ln \epsilon \quad (9)$$

where C and k are the linear and the exponential softening coefficients respectively. Since this equation is nonlinear in C it is not possible to find out both C and k using the principles of linear regression analysis. However in the neighbourhood of $C = C_0$ the equation 9 may be approximately represented by the first two terms of the Taylor's series as follows

$$\ln (\dot{\epsilon}/\dot{\epsilon}_1) = k \ln \epsilon + \ln (1 + C_0 \epsilon) + \left[\frac{\partial \ln (\dot{\epsilon}/\dot{\epsilon}_1)}{\partial C} \right] \Delta C \quad (10)$$

Equation 10 being linear in both k and ΔC it is possible to estimate each of these by the method of least squares. The term within the second bracket essentially represents the magnitude of the error as a result of an improper choice of C as C_0 and ΔC gives a measure of the change in the magnitude of C_0 which would provide a better estimate. Therefore by the repeating the process of computation with a new value of C given by

$$C = C_0 + \Delta C/\eta \quad (11)$$

where η is a constant, ΔC could be made negligibly small. Similar approach has been used earlier for estimating nonlinear stress rupture parameters⁽¹⁰⁾.

A computer program based on this principle has been developed to estimate both the linear and the exponential softening coefficients. This model first estimates an initial value of C assuming that only linear softening model is operating. It has been observed that this approach leads to a rapid convergence when η in equation 11 is 1. However a choice of $\eta = 2$ is recommended as it gives a smooth convergence.

Using this program the plots given in Figure 5 have been generated. Comparison with the experimental points clearly reveals that the present analysis provides a much better prediction. Once these two softening coefficients have been estimated it is now possible to simulate the creep curve by integrating the equations 1-3. The function f and g in this case should be given by

$$g(\omega) = f(\omega) = (1 + (C/k)\omega) \exp(\omega) \quad (12)$$

The predictions of the creep curves assuming exponential, linear and the combined model for a specific condition have been compared in Figures 4-5. As expected in this case the combined model gives a better prediction. Incorporation of the present analytical procedure therefore significantly improves predictive capability of the *crispen* package.

3. MODELLING CREEP BEHAVIOUR OF SINGLE CRYSTAL SUPERALLOYS

The creep behaviour of single crystal superalloys, like that of the simpler equiaxed wrought or cast versions is dominated by a progressively increasing creep rate over most of its life. Dyson and McLean⁽⁶⁾ have shown that for nickel base superalloys this extensive tertiary-creep behaviour is a result of strain softening probably due to the accumulation of mobile dislocations. This concept has been used in *crispen* to develop a physics based method of analysis of the creep curve so as to allow extrapolation or interpolation to arbitrary stress/temperature conditions. However the formalism used here implicitly assumes the material to be isotropic. This part of the report examines how the model could be extended to account for the inherent crystallographic anisotropy of single crystal superalloys.

3.1 Development of the Model

Ion et al (1) discuss two variants of the strain softening model that are associated with either linear or exponential accumulations of damage with creep strain. Recently, Maldini and Lupinc (11) have suggested that the linear strain softening model is more appropriate to single crystal superalloys and this conclusion is supported by Curtis et al (12) from analysis of an extensive creep database for a single crystal superalloy. Consequently, the following discussion will be restricted to extending the linear strain softening model. The exponential strain softening model can be similarly modified if required.

The variation in uniaxial creep rate $\dot{\epsilon}$ with increasing creep strain ϵ can be represented by the following equation (1, 6):-

$$\dot{\epsilon} = \dot{\epsilon}_1 (1 + C_3 \epsilon) \quad (13)$$

where $\dot{\epsilon}_1(\sigma, T)$ is the initial creep rate, σ is the applied axial stress, T is the temperature and C_3 is the strain softening coefficient. Curtis et al (12) have shown that for $\langle 001 \rangle$ crystals $\dot{\epsilon}_1(\sigma, T)$ is well described by an exponential, rather than power law, formulation of creep. Consequently, Equation 1 can be expressed more fully in the following form:-

$$\dot{\epsilon} = C_1 \exp \left[C_2 \sigma - \frac{Q_1}{RT} \right] (1 + C_3 \epsilon) \quad (14)$$

where C_1 , C_2 and C_3 are all material constants, Q_1 is the activation energy for creep and R is the gas constant.

The study also reveals that the softening coefficient C_3 as well can be represented by an expression given below:

$$C_3 = C_4 \exp \left[\frac{Q_2}{RT} - C_5 \sigma \right] \quad (15)$$

The axial strain ϵ is the resultant of shear strains γ due to all active slip systems in the crystal. Consequently, Equations 13-15 can be reformulated in terms of shear stresses (τ) and shear strains (γ) for appropriate slip systems to allow the simulation of creep along an arbitrary crystallographic direction. Thus, for nickel-base superalloys plastic deformation is thought to result from shear on one or a combination of the following slip systems: $\{111\}\langle\bar{1}\bar{1}0\rangle$, $\{111\}\langle\bar{1}\bar{1}2\rangle$ or $\{100\}\langle 011\rangle$. We now consider the formulation of Equation 14 when strain results from shear displacements on all possible slip systems of the arbitrary type $\{n_1 n_2 n_3\} \langle b_1 b_2 b_3 \rangle$.

Let γ^k be the magnitude of the shear on the k -th slip system represented by $(n_1^k n_2^k n_3^k) [b_1^k b_2^k b_3^k]$ where n_i^k and b_i^k represent the components of the unit vectors denoting the slip plane and slip direction respectively along the cubic crystallographic axes. As a result of such deformation, the crystallographic axes may rotate and the indices of the tensile axis may change. However, since the indices of the slip system are invariant, the sum of the displacement components with respect to the crystallographic axis is given by:-

$$\sum \epsilon_{1j}^k = \sum \gamma^k b_1^k n_j^k \quad (16)$$

The suffixes i, j in the above equation denote components along the crystal axes and can have integer values from 1 to 3. If $[t_1 t_2 t_3]$ and $[T_1 T_2 T_3]$ are the vectors representing the tensile axis before and after a small amount of deformation, it can be shown using the matrix method followed by Chin et al (13) that:-

$$\begin{bmatrix} T_1 \\ T_2 \\ T_3 \end{bmatrix} = \begin{bmatrix} 1 + \sum \epsilon_{11}^k & \sum \epsilon_{12}^k & \sum \epsilon_{13}^k \\ \sum \epsilon_{21}^k & 1 + \sum \epsilon_{22}^k & \sum \epsilon_{23}^k \\ \sum \epsilon_{31}^k & \sum \epsilon_{32}^k & 1 + \sum \epsilon_{33}^k \end{bmatrix} \begin{bmatrix} t_1 \\ t_2 \\ t_3 \end{bmatrix} \quad (17)$$

On differentiating Equation 16 with respect to time, recognising that the initial orientation is invariant one obtains:-

$$\begin{bmatrix} \dot{\epsilon}_1 \\ \dot{\epsilon}_2 \\ \dot{\epsilon}_3 \end{bmatrix} = \begin{bmatrix} \sum \dot{\epsilon}_{11}^k & \sum \dot{\epsilon}_{12}^k & \sum \dot{\epsilon}_{13}^k \\ \sum \dot{\epsilon}_{21}^k & \sum \dot{\epsilon}_{22}^k & \sum \dot{\epsilon}_{23}^k \\ \sum \dot{\epsilon}_{31}^k & \sum \dot{\epsilon}_{32}^k & \sum \dot{\epsilon}_{33}^k \end{bmatrix} \begin{bmatrix} t_1 \\ t_2 \\ t_3 \end{bmatrix} \quad (18)$$

where $\dot{\epsilon}_{ij}^k = \dot{\gamma}^k b_i^k n_j^k$ (19)

Expressions for $\dot{\gamma}^k$ can be obtained from Equation 14 by substituting the appropriate resolved shear stress τ^k for σ and the shear strain γ^k for ϵ .

$$\dot{\gamma}^k = C_1^k \exp \left[C_2^k \tau^k - \frac{Q_1}{RT} \right] (1 + C_3^k \gamma^k) \quad (20)$$

where $C_2^k = C_2 m^k$ and

$$C_3^k = C_4^k \exp \left[\frac{Q_2}{RT} - C_5^k \sigma \right] \quad (21)$$

m^k is the reciprocal of the Schmid factor for the k -th slip system. The constants C_1^k and C_3^k are related to C_1 and C_3 by a geometrical factor that can be determined from Equation 17. For the case of a [001] tensile axis and the {111}<1 $\bar{1}$ 0> slip system it can be shown that:-

$$\dot{\epsilon}_{\langle 001 \rangle} = \frac{8}{\sqrt{6}} \dot{\gamma}_{\{111\}\langle 1\bar{1}0 \rangle} \text{ and } \dot{\epsilon}_{\langle 001 \rangle} = \frac{8}{\sqrt{6}} \dot{\gamma}_{\{111\}\langle 1\bar{1}0 \rangle} \quad (22)$$

In this particular case, of the 12 possible slip systems 4 have a Schmid factor of zero and hence will not contribute to creep deformation. The remaining 8 have an identical Schmid factor of 0.4082 and hence each will make the same contribution to creep strain. However, if the slip system were {111}<1 $\bar{1}$ 2>, of the 12 possible slip systems, four have a Schmid factor of 0.4714 and the remaining 8 have much lower values of 0.2357. On the basis of Equation 20, the shear creep rate on these eight slip systems will be negligible in comparison to the 4 more highly stressed systems. In this case the relationship between $\dot{\epsilon}$ and $\dot{\gamma}$ can be shown to be:-

$$\dot{\epsilon}_{\langle 001 \rangle} = \frac{8}{3\sqrt{2}} \dot{\gamma}_{\{111\}\langle 1\bar{1}2 \rangle} \text{ and } \dot{\epsilon}_{\langle 001 \rangle} = \frac{8}{3\sqrt{2}} \dot{\gamma}_{\{111\}\langle 1\bar{1}2 \rangle} \quad (23)$$

Thus, by using Equations 20-22, the material constants used in the tensile formulation of tertiary creep of <001> oriented crystals can be converted to those needed for the shear formulation. With this information it is possible to simulate numerically the tensile creep of a single crystal of arbitrary orientation using Equations 17-20. A standard sub-routine

using the Runge-Kutta method with adaptive step size control (14) was used to integrate Equation 20; the solution was insensitive to the time interval used for the simulation.

3.2 Results and Discussion

Figure 6 shows a typical creep curve for a $\langle 001 \rangle$ oriented single crystal superalloy SRR99. Equation 14 has been fitted to these strain/time data using the methods described in reference 1 and 2 and the calculated curve is compared with the measured data in Figure 6. The constants for the tensile formulation can be transformed as described above to those required for shear formulation assuming either $\{111\}\langle 0\bar{1}1 \rangle$ or $\{111\}\langle \bar{1}\bar{1}2 \rangle$ slip respectively. The values of these constants for shear on $\{111\}\langle 1\bar{1}0 \rangle$ are listed in Table 3. The curves generated for these slip systems using shear formulation are included in Figure 6; the small discrepancies between the creep curves given by tensile and shear formulations at higher strains are a result of errors in the numerical integration and are well within the scatter associated with creep performance (15).

TABLE 3

MATERIAL CONSTANTS FOR CREEP OF SRR99 IN
TENSILE AND SHEAR FORMULATIONS

Parameters	Tensile Formulation		Shear Formulation		Unit
	$\langle 001 \rangle$	$\langle 111 \rangle$	$\{111\}\langle 1\bar{1}0 \rangle$	$\{100\}\langle 011 \rangle$	
C_1	9.3×10^{13}	2.53×10^{-5}	2.85×10^{13}	1.79×10^{-5}	s^{-1}
C_2	1.77×10^{-2}	5.57×10^{-3}	4.34×10^{-2}	1.18×10^{-2}	MPa^{-1}
C_4	1.36×10^{-2}	7.56×10^5	4.44×10^{-2}	1.07×10^6	
C_5	0.009	0.005	0.022	0.001	MPa^{-1}
Q_1	552	85.6	552	85.6	$kJmol^{-1}$
Q_2	131	- 82	131	- 82	$kJmol^{-1}$

NB $\dot{\epsilon}_1 = C_1 \exp(C_2 \sigma - Q_1/RT)$ and $C_3 = C_4 \exp(Q_2/RT - C_5 \sigma)$

Having established the appropriate constants for shear creep by analysis of creep data for the symmetrical $\langle 001 \rangle$ orientation, these can be used to generate tensile creep curves for arbitrary orientations. Figure 7 shows the creep curves computed for exact $\langle 001 \rangle$, $\langle 111 \rangle$ and $\langle 011 \rangle$ orientations assuming that slip occurs on $\{111\}\langle 0\bar{1}1 \rangle$ only. These are symmetrical orientations and there are no changes in orientations with strain. The model predicts that the creep performance of $\langle 001 \rangle$ is inferior to that of $\langle 011 \rangle$ which

is contrary to experience while $\langle 111 \rangle$ has the best creep behaviour in agreement with certain observations. However when a small deviation from $\langle 011 \rangle$ is considered large crystal rotations occur and this leads to a change in the order of creep performance for $\{111\}\langle 0\bar{1}1 \rangle$ slip as shown in Figure 7. This is at least consistent with the experimental observations of the anisotropy of creep performance.

The comparison of the creep curves of $\langle 111 \rangle$ SRR99 for the few test conditions under which data are available indicate that the predictions based on the shear formulation along $\{111\}\langle 0\bar{1}1 \rangle$ are negligible when compared with the actual plot. This indicates that certain other slip systems must be contributing to the creep along $\langle 111 \rangle$ axis. There is some experimental evidence that both octahedral and cube slip can occur in nickel base superalloys^(16,17). Indeed models of the anomalous temperature dependence of yield in intermetallic compounds, such as γ' which constitutes 70 vol% of SRR99, appeal to the occurrence of thermally activated cross slip onto cube planes. The database on the creep performance of $\langle 111 \rangle$ SRR99 is very limited to permit a reliable estimation of the material constants needed for the shear formulation along $\{100\}\langle 011 \rangle$. An approximate estimate of these may however be obtained from a set of available creep curves under different test conditions. Since the contribution of octahedral slip towards the creep of $\langle 111 \rangle$ oriented crystals were found to be insignificant attempts have been made to model its behaviour on the basis of the material constants for cube slip determined from those creep curves only. These constants are given in Table 3.

Figure 8 shows a typical creep curve of a $\langle 111 \rangle$ oriented SRR99 single crystal simulated on the basis of shear along $\{100\}\langle 011 \rangle$ as well as tensile formulation. Both of these describe the experimental data reasonably well. The small difference in the predictions between shear and tensile formulations is a result of numerical computation and is insignificant when compared with the scatter associated with creep performance.

Having established the set of material constants for shear creep on $\{100\}\langle 011 \rangle$ as well from $\langle 111 \rangle$ oriented crystals it is possible to generate the creep curve for any arbitrary orientation when both octahedral and cube slip operate. Figure 9 presents a set of creep curves for different orientations when both slip systems are in operation. These represent the experimental plots well within the scatter associated with creep performance. Comparison with the plots predicted on the basis of octahedral slip reveal that the introduction of the concept of cube slip significantly reduces the degree of anisotropy.

Using this approach it is now possible to predict the creep performance of crystals of any orientation and represent the same in the form of contour maps over the entire stereographic triangle. Some of these have been presented in Figure 10. This shows that crystals near $\langle 001 \rangle$ have the best creep resistance when deformation takes place by both

octahedral and cube slip. This trend is indeed in agreement with most experimental observations available to date. However the present prediction is based on a very limited database on $\langle 111 \rangle$ crystal. There is a need to collect more data on the creep performance of SRR99 along $\langle 111 \rangle$ orientation to enable a more precise estimation of the material constants for cube slip.

4. UNIFIED MODEL

Development of a unified constitutive model for creep and plasticity has been an area of great interest over the last two decades (18-24). The main impetus for R&D efforts came from the possibility of this approach being incorporated into finite element codes for the design and analysis of structures. This objective has yet to be achieved for a number of reasons: those often quoted are the mathematical stiffness of the equations used - which affect accuracy of calculations; and the incorporation of a large number of necessary variables into the model, which are difficult to evaluate (23,24).

While developing a constitutive model it is often necessary to identify and select only a few of the most important aspects of the material behaviour. Any attempt to condense all aspects often lead to a large number of complex equations which are difficult to solve. Most of the current models (18-24) place great emphasis on the hardening behaviour of the material encountered during the primary stage of creep as in many pure metals and single phase alloys. However many engineering materials such as the superalloys exhibit a prominent strain softening behaviour right from the early part of its creep life. Therefore constitutive equations which describe this aspect of the material behaviour will be most appropriate for superalloys.

Application of the cristen package has been shown to explain the creep behaviour of a number of superalloys fairly well. In many of these the intrinsic softening mechanism has been found to follow the linear model. Therefore the following constitutive equations are sufficient to simulate their creep behaviour⁽¹⁾.

$$\begin{aligned}\dot{\epsilon} &= \dot{\epsilon}_1 (1 - S) (1 + \omega) \\ \dot{S} &= H\dot{\epsilon} - RS \\ \dot{\omega} &= C\dot{\epsilon}\end{aligned}\tag{24}$$

Where the set of four parameters representing base creep rate ($\dot{\epsilon}_1$), coefficients of hardening (H), recovery (R) and softening (C) may vary with stress and temperature. This section examines how these equations could be used to model other forms of uniaxial mechanical tests. The exponential or the time softening models can also be similarly

modified if required.

4.1 Development of the Model

In order to model creep tests it was not necessary to constitute a differential equation representing the applied stress since it remains constant. Besides ϵ in the above equation was used to denote the plastic strain (ϵ_p) even though the total strain (ϵ) is known to be made up of the elastic (ϵ_E) and the plastic (ϵ_p) components. In a creep test this is immaterial as $\epsilon_E \ll \epsilon_p$. However this does not hold in other forms of mechanical tests. Therefore to extend the present approach to model other forms of uniaxial tests we must replace ϵ in equation 24 by ϵ_p and build up an equation representing applied stress σ on the assumption that it is proportional to the elastic strain. Thus the constitutive model for all forms of mechanical tests on superalloys could be given by

$$\begin{aligned}\dot{\epsilon}_p &= \dot{\epsilon}_i (1 - S) (1 + \omega) \\ \dot{S} &= H \dot{\epsilon}_p - RS \\ \dot{\omega} &= C \dot{\epsilon}_p \\ \dot{\sigma} &= E (\dot{\epsilon} - \dot{\epsilon}_p)\end{aligned}\tag{25}$$

where E is the Young's modulus. The above set of four coupled differential equations can be used to simulate any uniaxial mechanical test provided appropriate boundary conditions are selected and the assumption that all tests are subject to the same damage mechanisms is valid. For example in the case of a constant strain rate test, $\dot{\epsilon}$ is directly proportional to the cross head speed of the testing machine and in a stress relaxation test $\dot{\epsilon} = 0$. Figure 12 provides a summary of the constitutive model and the boundary conditions for all such tests. These may be classified into two groups depending on the control procedure adopted during the tests. In a strain controlled test it is the total strain (ϵ) which is given by a simple function of time. Whereas in a load controlled test it is the applied stress that follows similar time dependence.

With this formulation it is possible to simulate numerically any forms of uniaxial mechanical tests. A standard sub-routine using the Runge-Kutta method with adaptive step size control was used to integrate the above equations. A user friendly interactive computer program has been developed. This has been used to simulate different types of strain and load controlled tests on IN738DS superalloy (1).

The material constants required for this have been obtained from the existing database on creep test at 850°C only. $\dot{\epsilon}_i$ has been assumed to follow a power law dependence;

$$\dot{\epsilon}_i = A \sigma^n\tag{26}$$

where A and n are material constants. Actual functional form of S which represents the hardening response is given in equations (1-2). The ratio σ^*/σ which is a measure of the limiting internal stress that builds up in the material has also been assumed to be a material constant (R_0). The values of the material constants used for the simulation are given in Table 4.

TABLE 4
MATERIAL CONSTANTS FOR IN738DS AT 850°C

A	4.2×10^{-35}	s^{-1}
n	10.7	
H	8×10^4	MPa
E	1.5×10^5	MPa
R_0	0.9	
C	20	

4.2 Results and Discussion

Figure 13 presents a set of predicted stress vs strain plot for IN738DS at 850°C under different strain rates. The plot exhibits that the stress increases with strain until a peak value is reached and there after it continues to decrease. In a normal stress-strain diagram this drop is usually associated with a localised deformation or necking. The present model however does not include the contribution of necking on creep. Therefore the predicted drop in the flow stress after the peak is due the effect of the intrinsic softening of the alloy. As expected the peak stress is found to be a function of the strain rate, and its magnitude is of the same order as the applied stress required to produce the same initial strain (or creep) rate in a constant stress creep test.

Figure 14 shows stress relaxation plots for IN738DS at 850°C at two different initial stress levels. The prediction shows that under all conditions the stress approaches a limiting value. In fact the trend is similar to those observed in many superalloys. Some experimental work have just been undertaken to check the validity of such predictions.

The stress-strain plots can also be predicted under cyclic loading through zero using this method. Figure 15 show such plots under two different strain rates. These tests have been simulated under strain control mode. Figure 16 shows how the stress is expected to change during the first few cycles. The analysis shows that the material exhibits very little cyclic hardening during the initial stage. This is followed by a prolonged stable

cyclic behaviour. Subsequently as the damage builds up the maximum stress in each successive cycle continues to drop. Figure 17 shows the nature of the elastic strain range vs the number of cycle plot. The plastic strain range increases with cycle and it exceeds the elastic strain range in this case right from the beginning. Nickel base superalloys such as IN738 is known to exhibit similar behaviour.

Similar σ vs ϵ plots have also be generated to simulate tests performed under load controlled conditions. These have been presented in Figures 18-20. These plots clearly indicate the condition underwhich the alloy is likely to undergo cyclic deformation without significant accumulation of plastic strain. The present analysis reveals that the chance of getting such a response increases as the mean stress approaches zero. Some results on austenic stainless steel does show similar behaviour.

Numerical solution of the constitutive equation (25) representing the high temperature deformation behaviour of nickel base superalloy does provide a means of simulating its response to a more complex form of loading than that encountered in a creep test. The nature of the plots simulated by this technique is similar to those reported for several nickel base superalloys. There is a need to undertake more experimental work on IN738DS under various test conditions to examine how close are the predictions obtained purely on the basis of the material constants derived from simple creep tests.

5. CONCLUSIONS

- (i) A method of estimating the linear and the exponential softening coefficients when both mechanisms operate in parallel has been developed and it has been incorporated in the MODSEL module of CRISPEN.
- (ii) The model based approach of CRISPEN has been extended to incorporate crystallographic anisotropy of deformation. The computer program developed on this approach is capable of simulating creep curves of crystals having any arbitrary orientation.
- (iii) It is necessary to consider the contribution from cube slip to explain the observed creep behaviour of SRR99 crystals having $\langle 111 \rangle$ orientation.
- (iv) Material constants for octahedral slip in SRR99 can be estimated from the creep curves of $\langle 001 \rangle$ oriented crystal whereas those for cube slip can be obtained from the creep curves of crystals having $\langle 111 \rangle$ orientation.
- (v) The above approach provides a means of mapping the creep performance of SRR99 superalloy crystals of all possible orientation.
- (vi) The unified model described above extends the CRISPEN approach to simulate other forms of mechanical tests such as constant strain rate, strain relaxation and low cycle fatigue. The predictions based on this method have been shown to describe most of the important features of these tests. However it is necessary to undertake experimental work to check the validity of the prediction.

ACKNOWLEDGEMENTS

The author was on deputation from October 1988 to October 1989 from the National Metallurgical Laboratory, Jamshedpur, India and was supported by an Overseas Development and Technical Cooperation Training Award administered by the British Council. He records his deep sense of appreciation to Dr Malcolm McLean for his inspiring guidance and supervision. He would like to thank Dr Brian Dyson, Dr Richard Curtis and Dr Ana Barbosa for helpful discussions and Dr M K Hossain, Superintendent, Division of Material Applications, NPL for providing the facility. Encouragement received from Professor S Banerjee, Director, National Metallurgical Laboratory, Jamshedpur during various stages of the work is also gratefully acknowledged.

REFERENCES

1. J C Ion, A Barbosa, M F Ashby, B F Dyson and M McLean, NPL Report DMA A115, April 1986.
2. A Barbosa, N G Taylor, M F Ashby, B F Dyson and M McLean, Proceedings of 6th International Symposium on Superalloys, edited by D N Duhal et al, 1988, The Metallurgical Society of AIME, Warrendale, Pennsylvania.
3. M Maldini, A Barbosa, B F Dyson and M McLean, NPL Report DMA A126, January 1987.
4. M F Ashby, and B F Dyson, NPL Report, DMA(A)77, March 1984.
5. B F Dyson, Review Phys. Appl. 23, 605-613, 1988.
6. B F Dyson and M McLean, Acta. Met., 31, 17, 1983.
7. R A Mackay, R L Dreshfield and R D Maier, Proceedings of 4th International Symposium on Superalloys, edited by J K Tien et al, 1980, Metals Park, Ohio, ASM.
8. D M Shah and D N Duhal, Proceedings of the 5th International Symposium on Superalloys, edited by M Gell et al, 1984, The Metallurgical Society of AIME, Warrendale, Pennsylvania.
9. P Caron, Y Ohta, Y G Nakagawa and T Khan, Proceedings of 6th International Symposium on Superalloys, edited by D N Duhal et al, 1988, The Metallurgical Society of AIME, Warrendale, Pennsylvania.
10. J B Conway, "Stress Rupture Parameters - origin, calculation and use", Gordon and Beach, London (1969), p 278.
11. M Maldini and V Lupinc, Scripta. Metall., 22, 1737, 1988.
12. R Curtis, R N Ghosh, P N Quested and M McLean - unpublished work.
13. G Y Chin, R N Thurston and N E A Nesbitt - Trans. AIME 239, 69, (1966).

14. W H Press, B P Flammery, S L Teukolsky and W T Vetterling, "Numerical Recipes - The Art of Scientific Computing", Cambridge University Press, Cambridge (1987) p 547.
15. R N Ghosh and M McLean, *Scripta Met.*, 23, 1301-1306 (1989).
16. B H Kear and B J Pearcy, *Trans. AIME* 239, 1209 (1967).
17. V Paidar, D P Pope and V Vitek, *Acta. Meta.*, 32, 435, (1982).
18. E W Hart, *Acta. Met.*, 18, 599, 1970.
19. Alan K Miller and Oleg D Sherby, *Acta. Met.*, 26, 97, 1976.
20. A Miller, *J Engg Materials Tech.*, (H) 96, 97, 1976.
21. U F Kocks, in *Unified Constitutive Equations for Creep and Plasticity*, ed. Alan K Miller, 1, 1987, (Elsevier Applied Science).
22. Alan K Miller, *idem*, 139.
23. D Bammann and R D Krieg, *idem*, 303.
24. A K Miller and T G Tanaka, *J. Eng. Mater. Tech.* H110, 205, 1988.

FIGURES

- Figure 1 Definition of an engineering parameter set (Table 1) that describes the shape of a creep curve and its dependence on stress and temperature.
- Figure 2 Types of strain rate ($\dot{\epsilon}$) vs strain (ϵ) plots which may be used to identify the dominant softening mechanisms in superalloys and estimate the softening coefficient. (a) exponential model (b) linear model. The slope in either cases gives the respective softening coefficient. NB $cr = \dot{\epsilon}$, $mcr = \dot{\epsilon}_i$.
- Figure 3 Typical creep curves predicted on the basis of either linear or exponential softening mechanisms. The points represent experimental plot. (a) exponential model (b) linear model ($cr = \dot{\epsilon}$, $mcr = \dot{\epsilon}_i$).
- Figure 4 A typical strain rate vs strain plot for IN738DS under conditions where both linear and exponential mechanisms operate in parallel. The points represent experimental data. (a) exponential model (b) linear model. None of the two gives a satisfactory fit ($cr = \dot{\epsilon}$, $mcr = \dot{\epsilon}_i$).
- Figure 5 (a) A typical creep curve for IN738DS simulated on the assumption that both exponential and linear softening mechanisms operate in parallel. The points represent experimental data. (b) The strain rate vs strain plot used to determine the linear and the exponential softening coefficients ($cr = \dot{\epsilon}$, $mcr = \dot{\epsilon}_i$).
- Figure 6 Creep curve for $\langle 001 \rangle$ oriented SRR99 tested at 1000°C and 300 MPa and the calculated creep curves for (a) tensile formulation (equation 14) and shear formulations for (b) $\{111\}\langle \bar{1}\bar{1}2 \rangle$ slip (equation 20).
- Figure 7 Calculated creep curves for SRR99 at 950°C and 300 MPa for axial stressing of crystals with exact $\langle 001 \rangle$, $\langle 011 \rangle$ and $\langle 111 \rangle$ orientations and for $\langle 067 \rangle$ and $\langle 2\ 12\ 13 \rangle$ orientations assuming only $\{111\}\langle \bar{1}\bar{1}0 \rangle$ slip.
- Figure 8 Creep curve for $\langle 111 \rangle$ oriented SRR99 tested at 950°C , 300 MPa and the calculated creep curves for (a) tensile formulation (Equation 14) and (b) shear formulations for $\{111\}\langle \bar{1}\bar{1}0 \rangle + \{100\}\langle 011 \rangle$ slip.
- Figure 9 Calculated creep curves for SRR99 at 850°C and 450 MPa assuming that slip takes place on both $\{111\}\langle \bar{1}\bar{1}0 \rangle$ and $\{100\}\langle 011 \rangle$. The respective constants were derived from $\langle 001 \rangle$ and $\langle 111 \rangle$ oriented crystals.

- Figure 10 A set of creep performance maps for SRR99 at 850°C, 400 MPa showing the time to reach a specific strain as a function of orientation.
- Figure 11 A set of creep performance maps for SRR99 at 850°C 400 MPa showing the levels of plastic strain attained at a specific time as a function of orientation.
- Figure 12 A unified constitutive model for uniaxial mechanical tests.
- Figure 13 A set of calculated stress vs strain curves for IN738DS at 850°C under different strain rates.
- Figure 14 A set of stress relaxation curves for IN738DS at 850°C calculated using the unified model and the material constants obtained from creep tests.
- Figure 15 Stress vs strain plot during the first few cycles of a strain controlled LCF test on IN738DS at 850°C calculated on the basis of the unified model using the material constants derived from creep tests, at two different strain rates (EDOT). (a) 1×10^{-2} (b) 1×10^{-3} per sec.
- Figure 16 Stress vs time plot during the first few cycles of a strain controlled LCF test on IN738DS at 850°C at two different strain rates. (a) 1×10^{-2} (b) 1×10^{-3} per sec.
- Figure 17 The elastic and the plastic strain ranges plotted as a function of the number of cycles during a computer simulated strain controlled LCF test on IN738DS at 950°C and two different strain rates (EDOT). (a) 1×10^{-2} (b) 1×10^{-3} per sec.
- Figure 18 (a) Stress vs strain plot during the first few cycles of a load controlled LCF test on IN738DS at 850°C calculated on the basis of the unified model using the material constants derived from creep tests. (b) Strain vs time under the above condition. At a mean stress of zero the material tends to approach a state of cyclic stability.
- Figure 19 (a) and (b) as in figure 18 but for mean stress < zero. The strain continues to decrease indefinitely with each cycle.
- Figure 20 (a) and (b) as in figure 18 but for mean stress > zero. The strain continues to increase indefinitely with each cycle.

Figure 21 The elastic and the plastic strain ranges plotted as a function of the number of cycles during a computer simulated load controlled LCF test on IN738DS at 850°C. (a) Mean stress is negative. (b) Mean stress is zero. (c) Mean stress is positive.

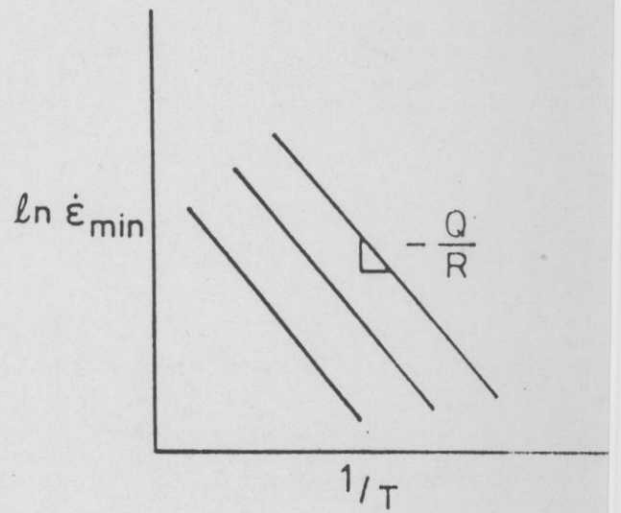
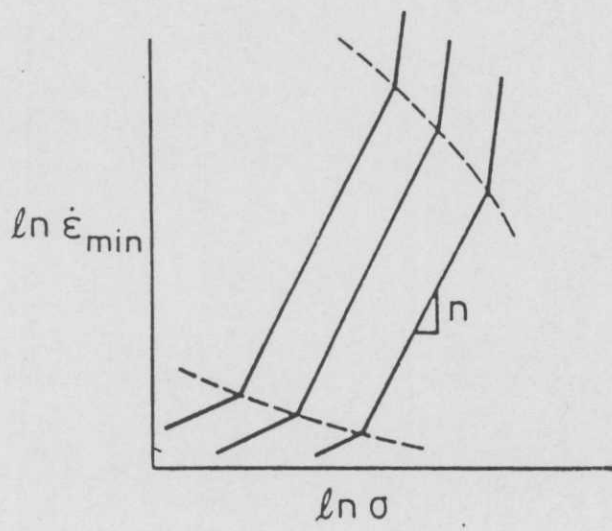
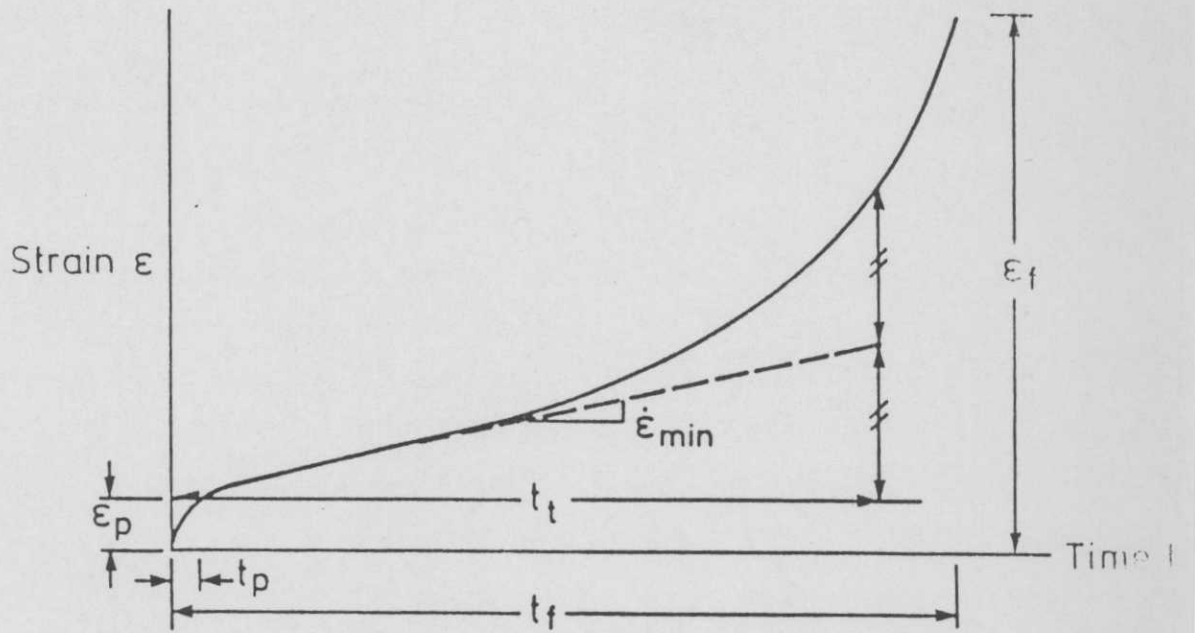


Fig 1

Test of exponential strain softening hypothesis !

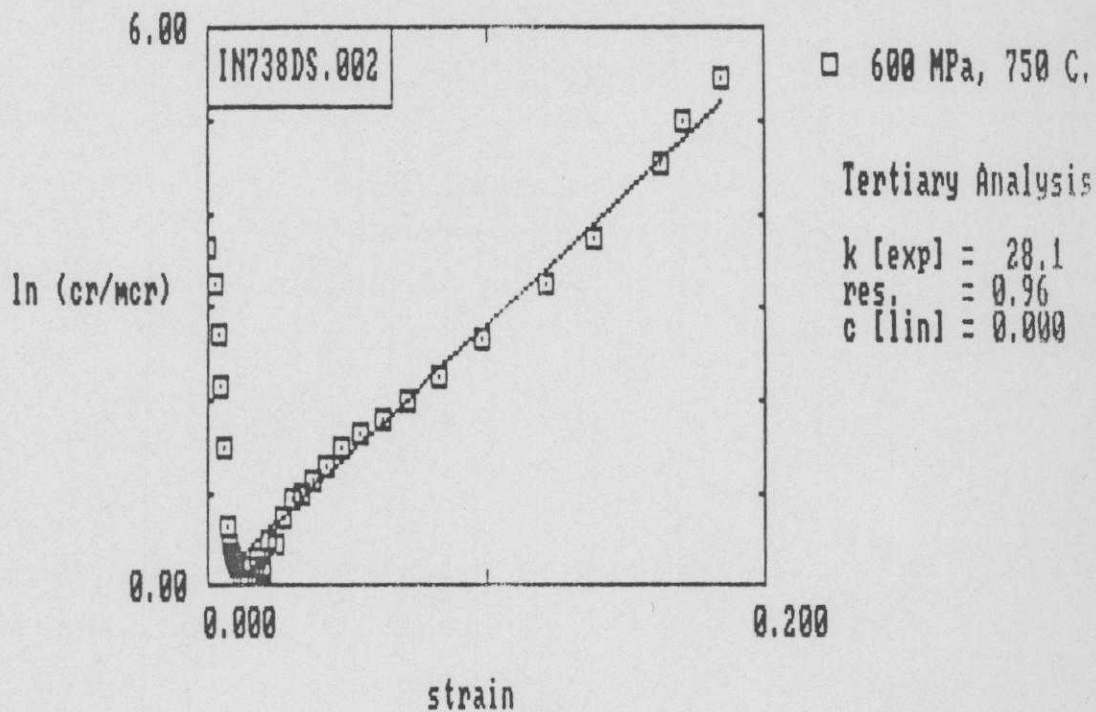


Fig 2a

Test of linear strain softening hypothesis !

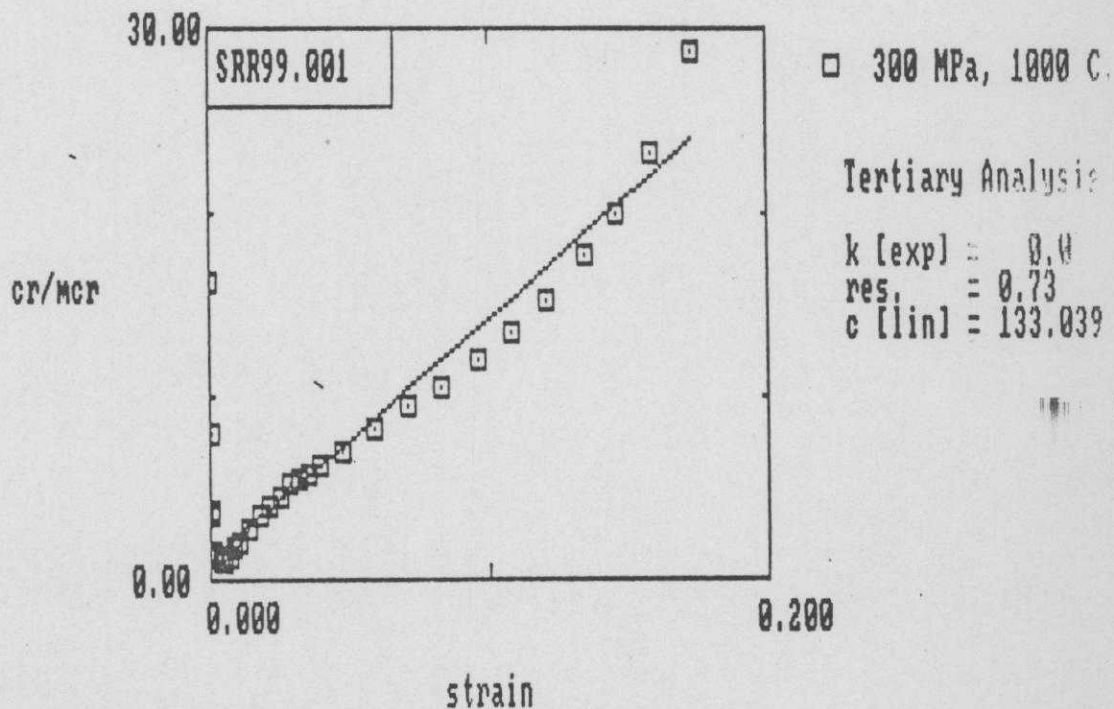


Fig 2b

Comparison of predicted and experimental creep curves.

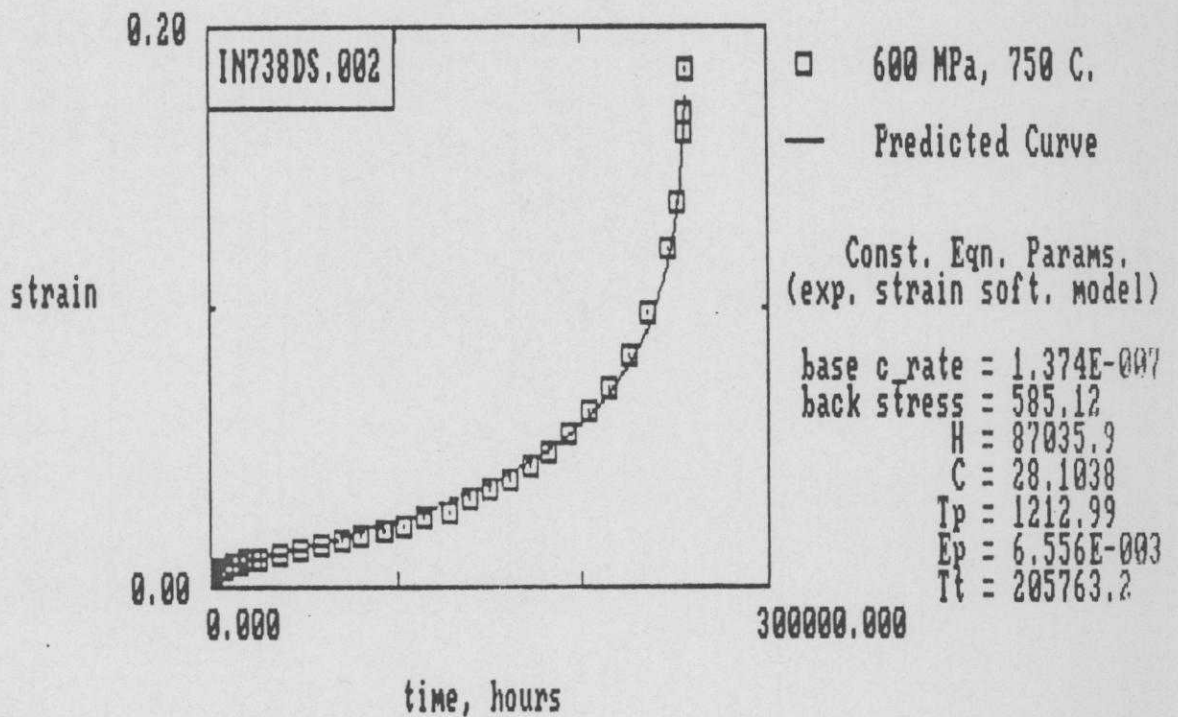


Fig 3a

Comparison of predicted and experimental creep curves.

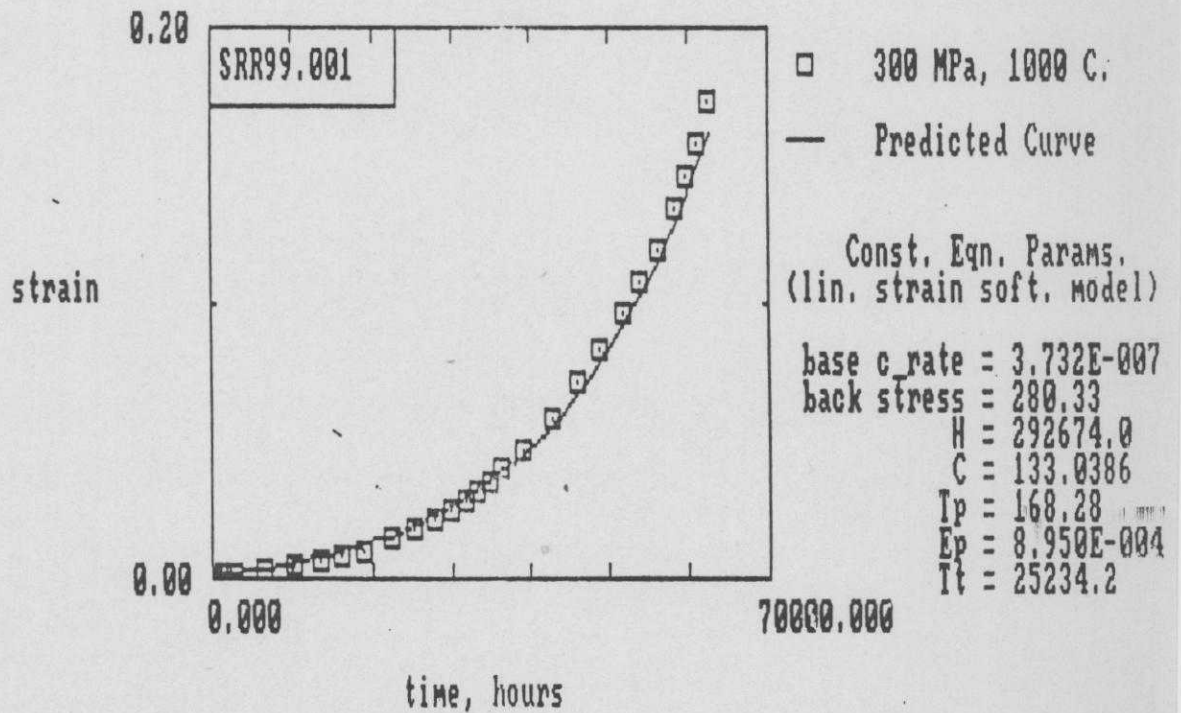


Fig 3b

Test of exponential strain softening hypothesis !

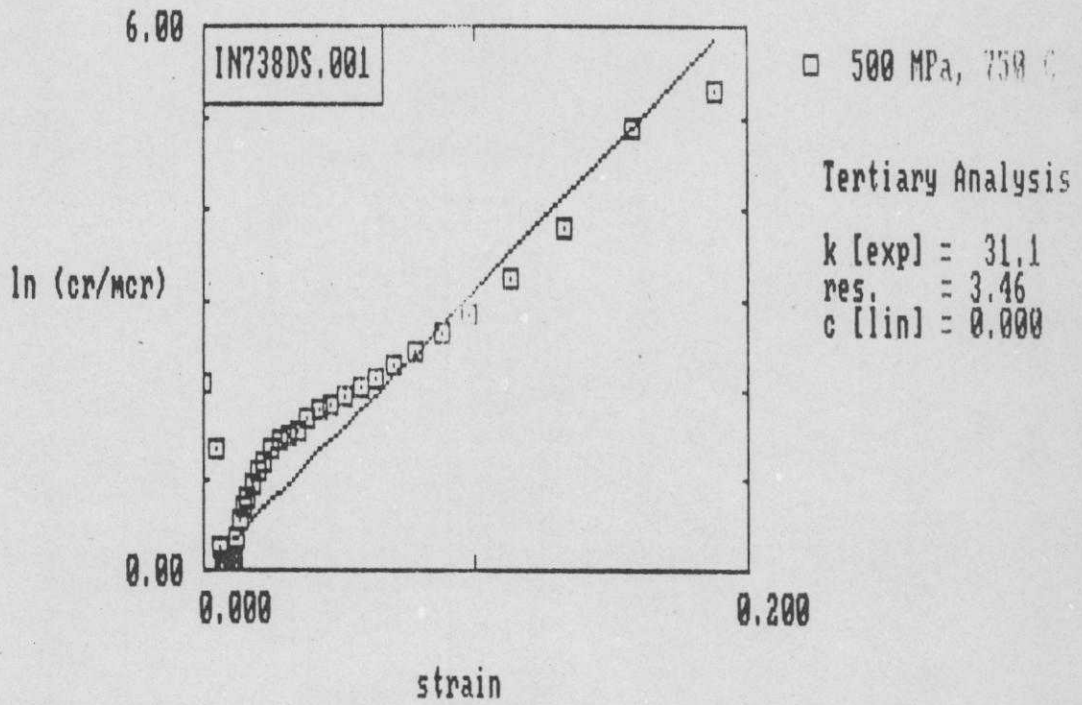


Fig 4a

Test of linear strain softening hypothesis !

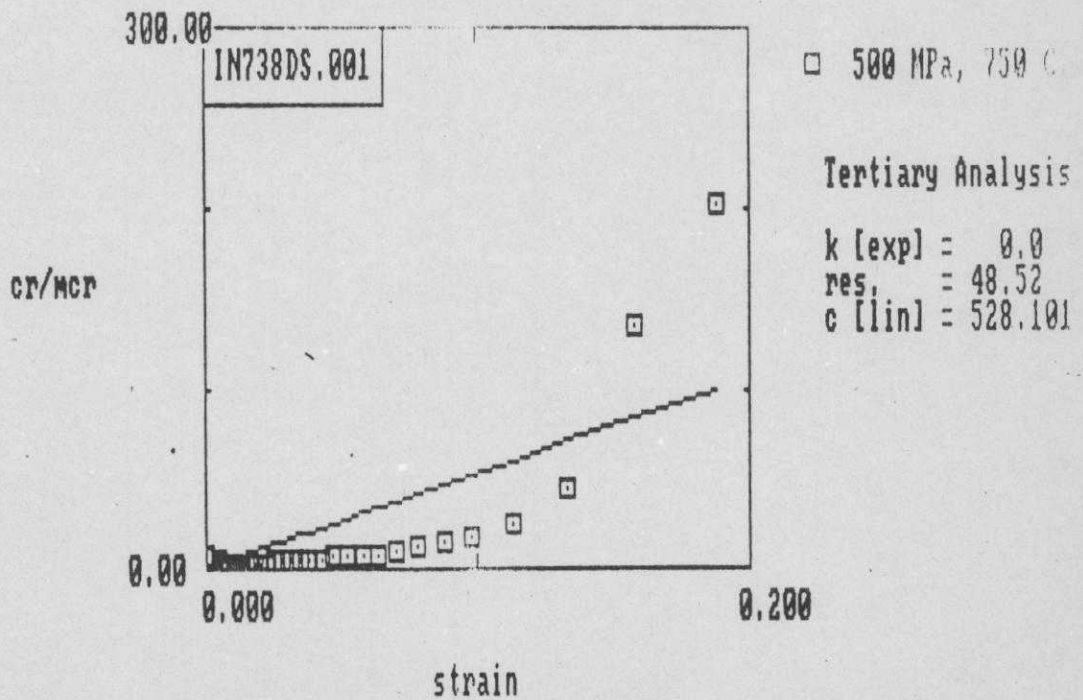


Fig 4b

Test of linear + exponential softening hypothesis !

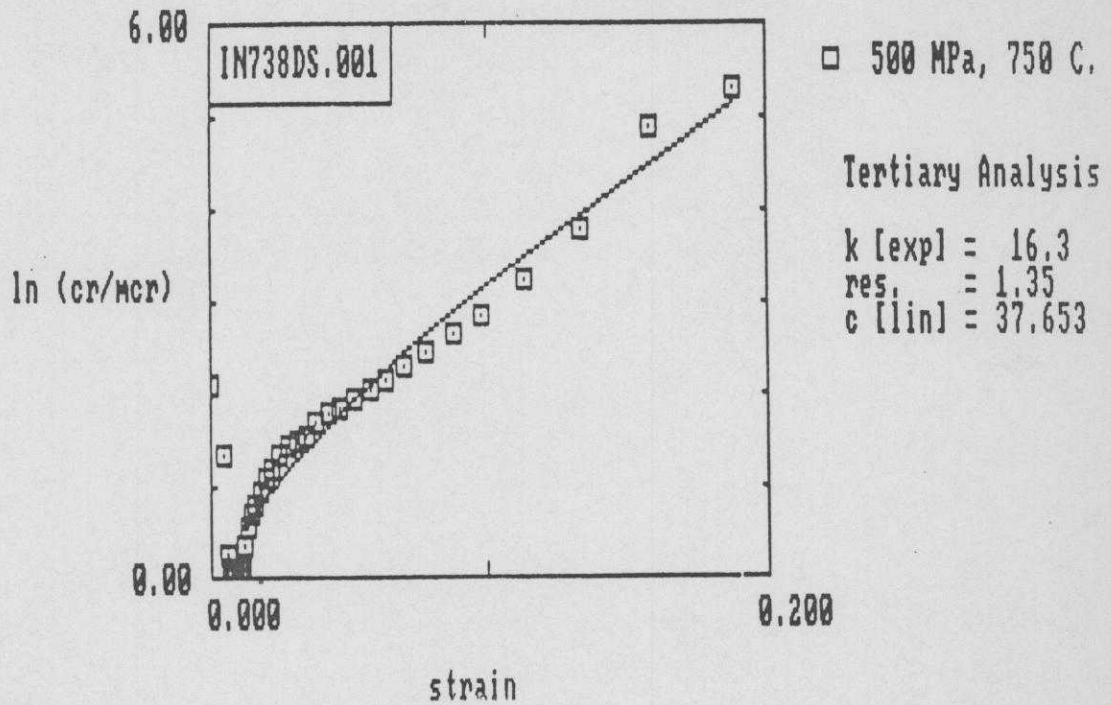


Fig 5a

Comparison of predicted and experimental creep curves.

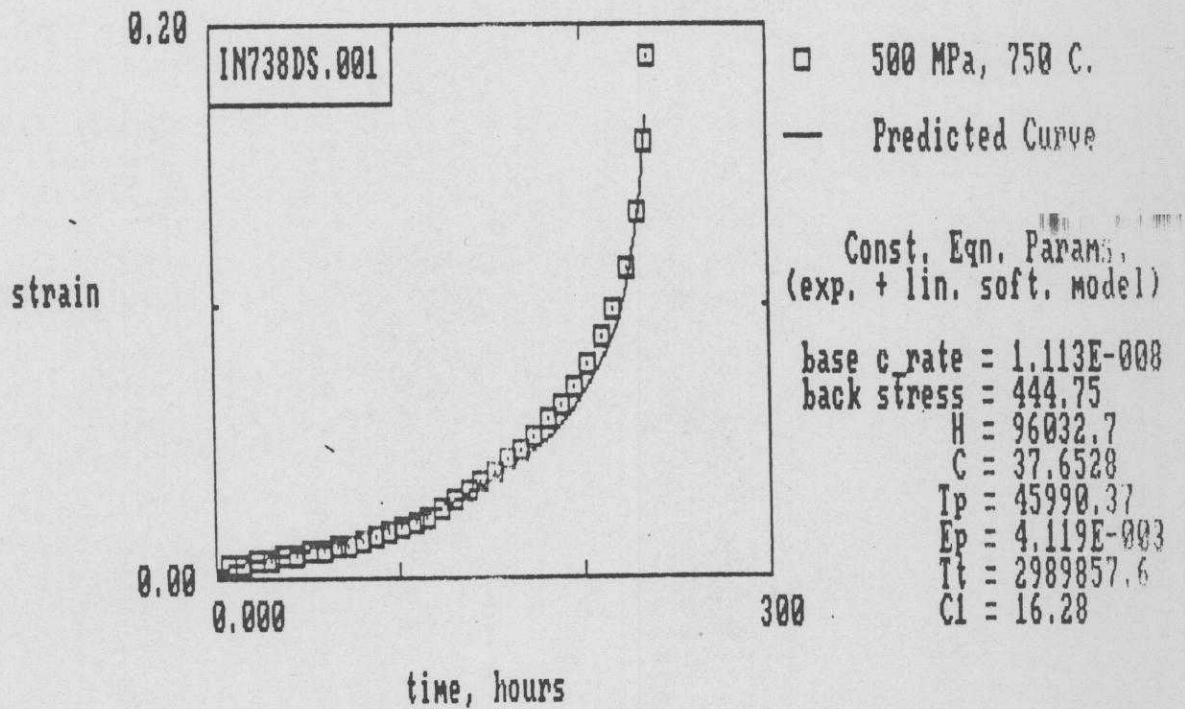


Fig 5b

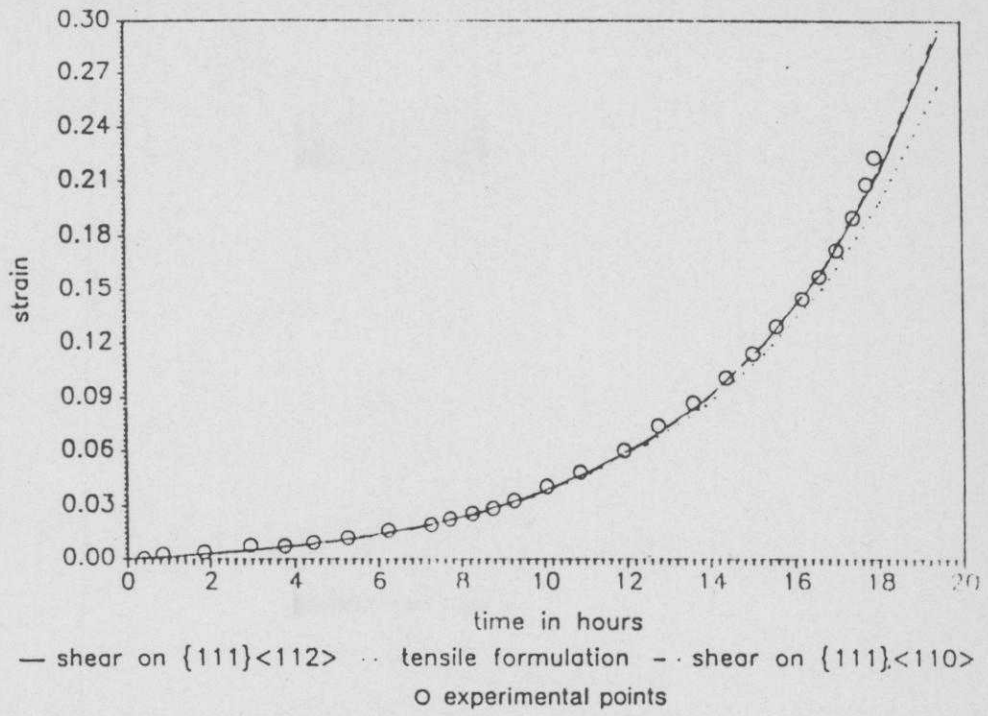


Fig 6

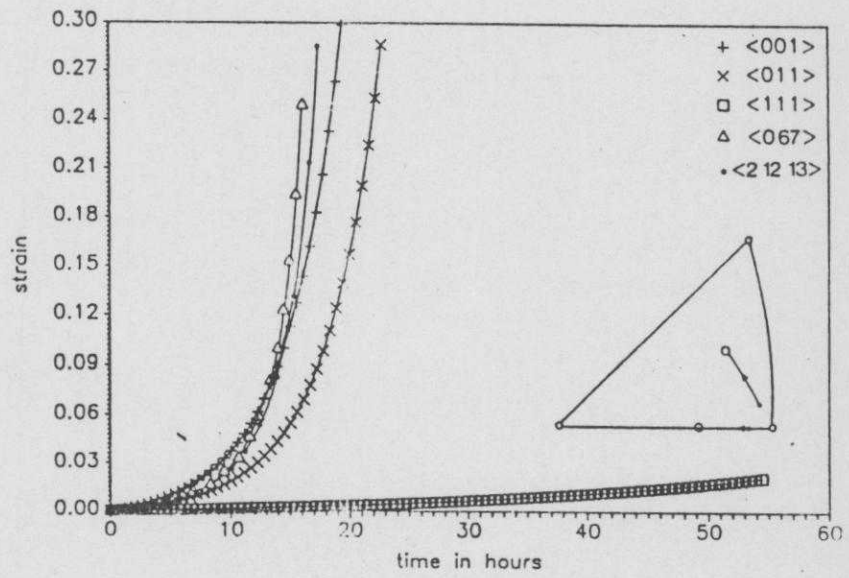


Fig 7

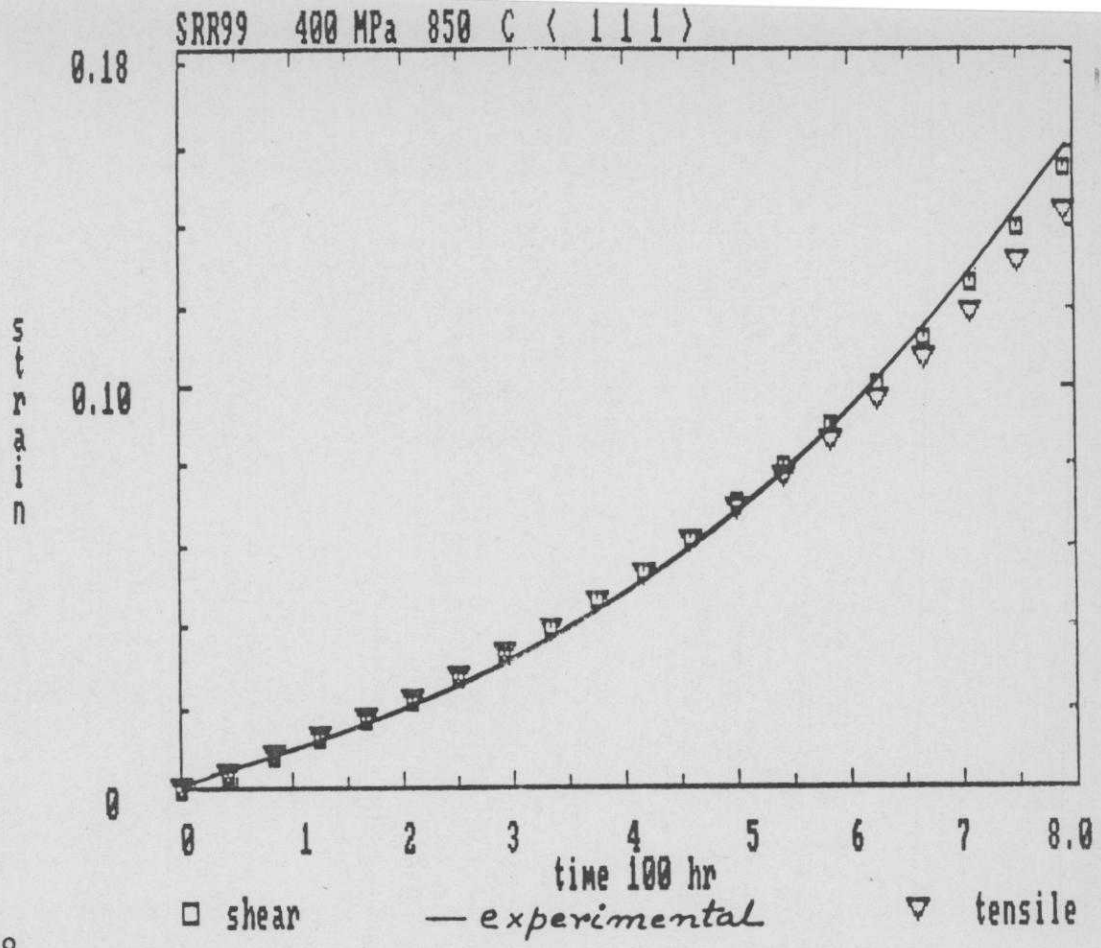


Fig 8

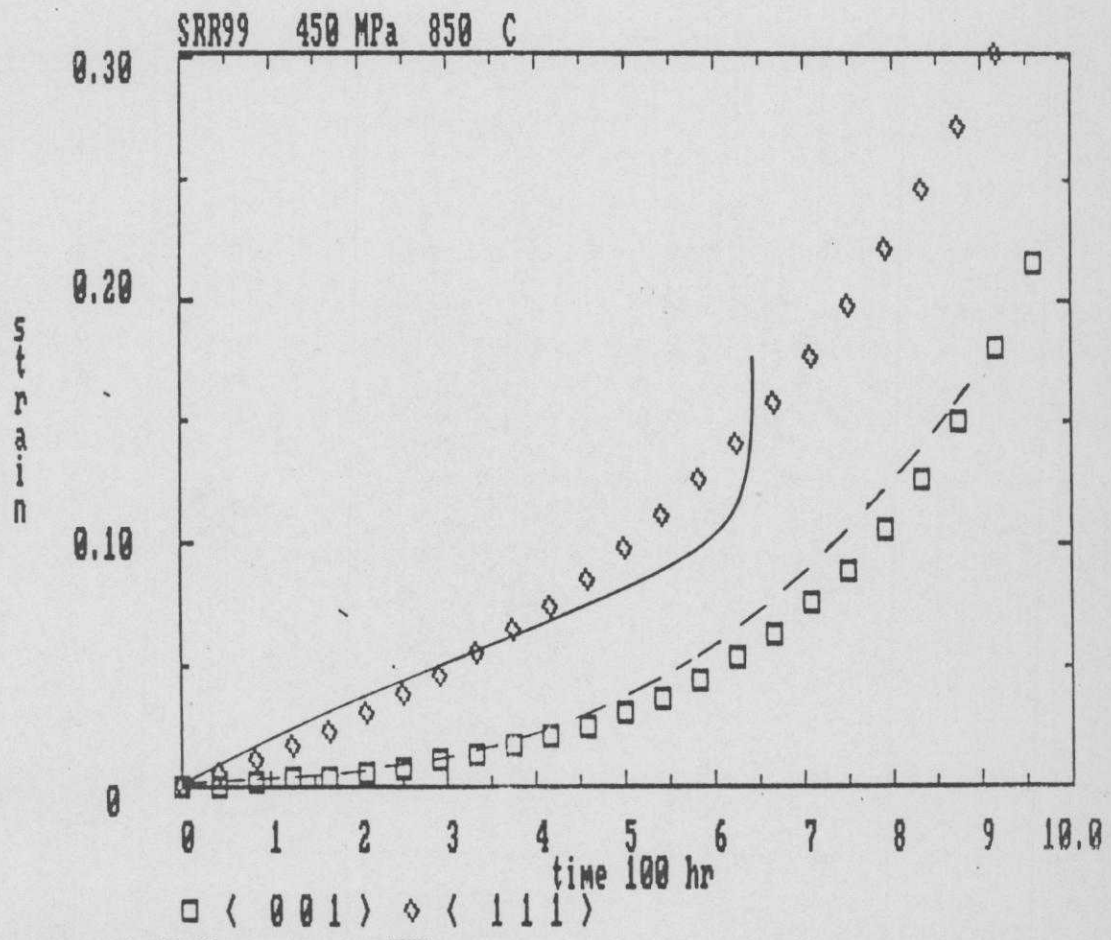


Fig 9

time to reach a strain of 0.10

□	1.8E+006 - 2.7E+006	sec
◇	2.7E+006 - 3.6E+006	sec
×	3.6E+006 - 4.5E+006	sec
+	4.5E+006 - 5.4E+006	sec
▽	5.4E+006 - 6.3E+006	sec
△	6.3E+006 - 7.2E+006	sec

stress = 400 MPa
temp = 850 deg, C
{111}<110>+{100}<110>

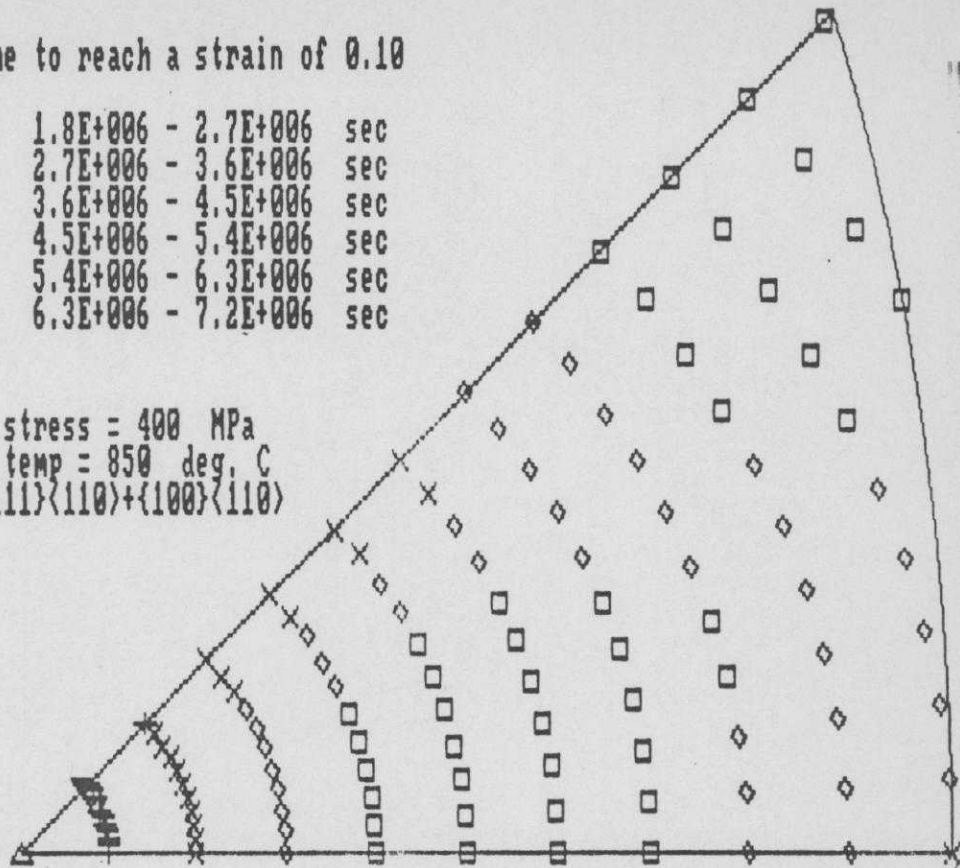


Fig 10a

time to reach a strain of 0.14

□	1.8E+006 - 2.8E+006	sec
◇	2.8E+006 - 3.8E+006	sec
×	3.8E+006 - 4.8E+006	sec
+	4.8E+006 - 5.8E+006	sec
▽	5.8E+006 - 6.8E+006	sec
△	6.8E+006 - 7.8E+006	sec

stress = 400 MPa
temp = 850 deg, C
{111}<110>+{100}<110>

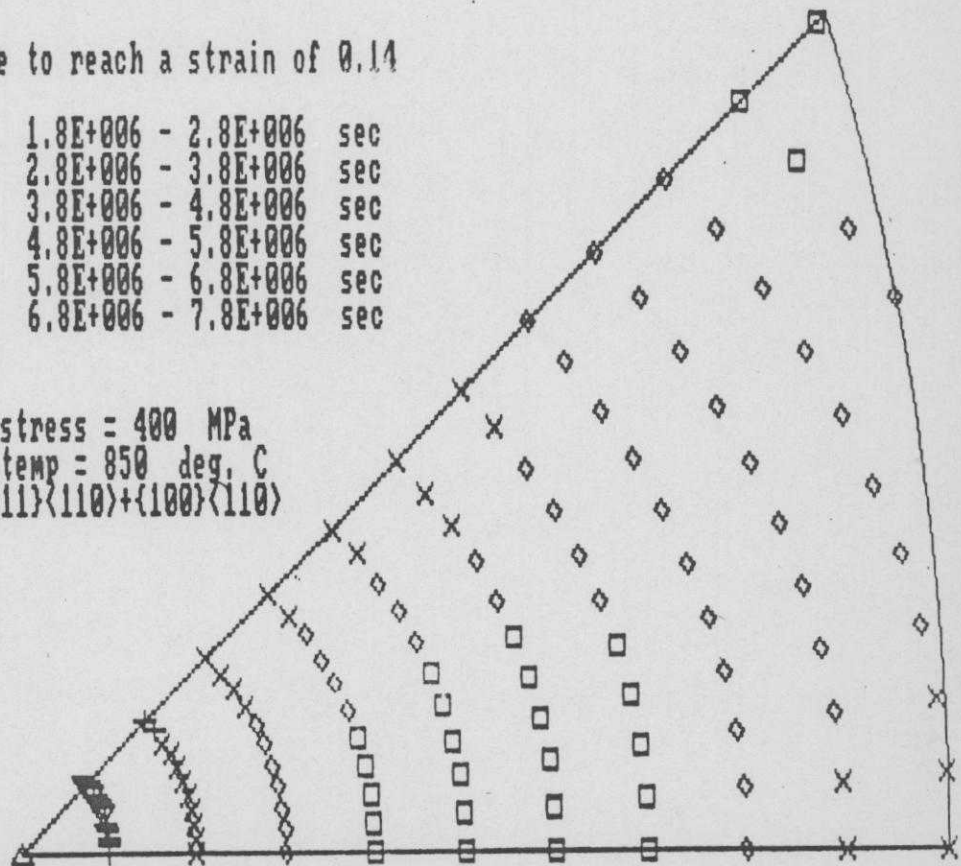


Fig 10b

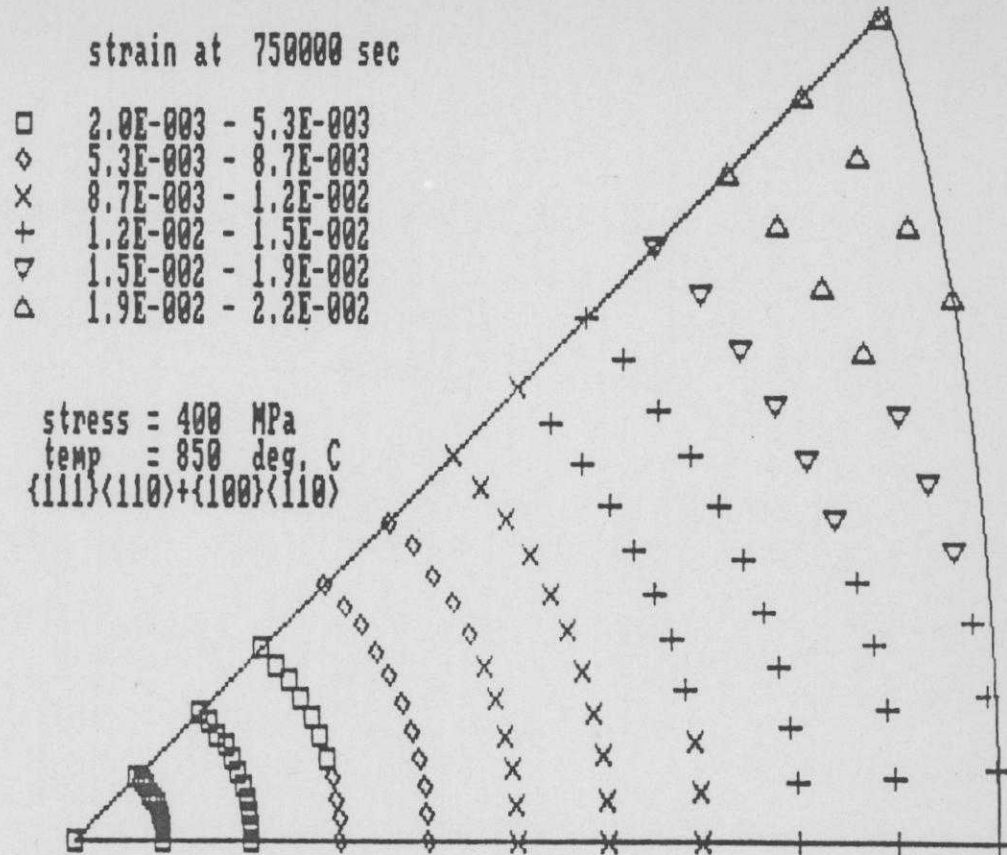


Fig 11a

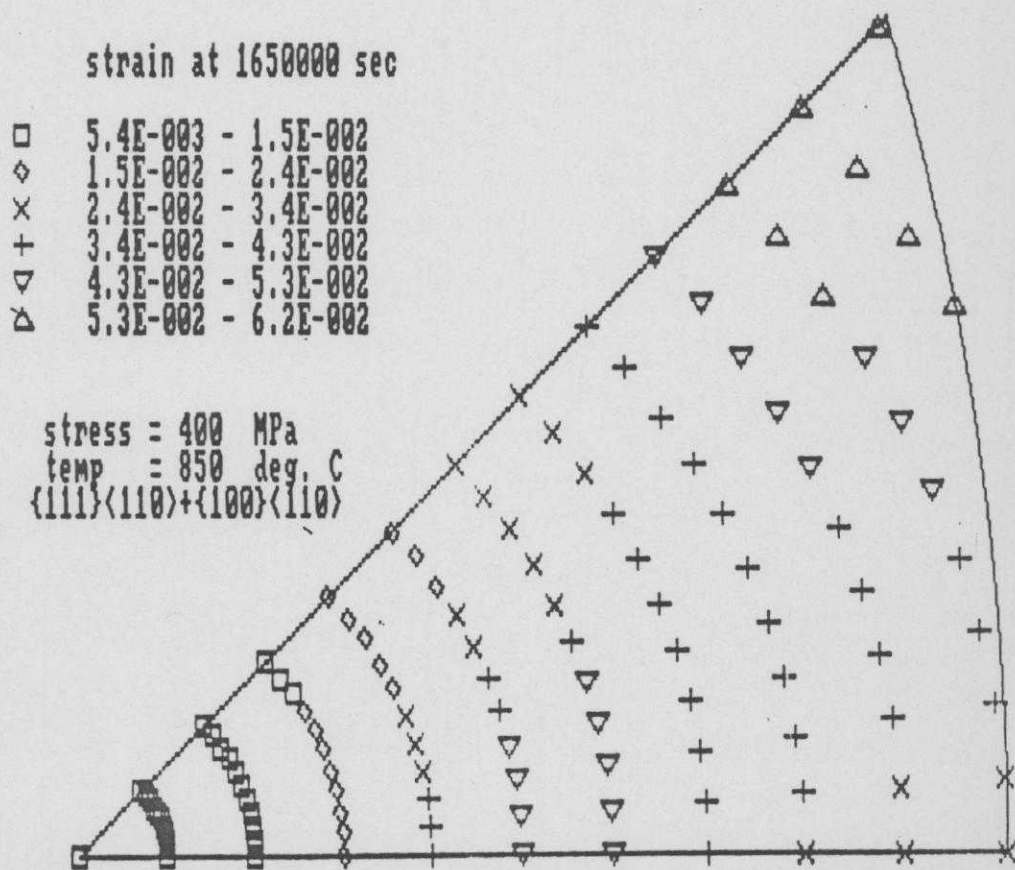


Fig 11b

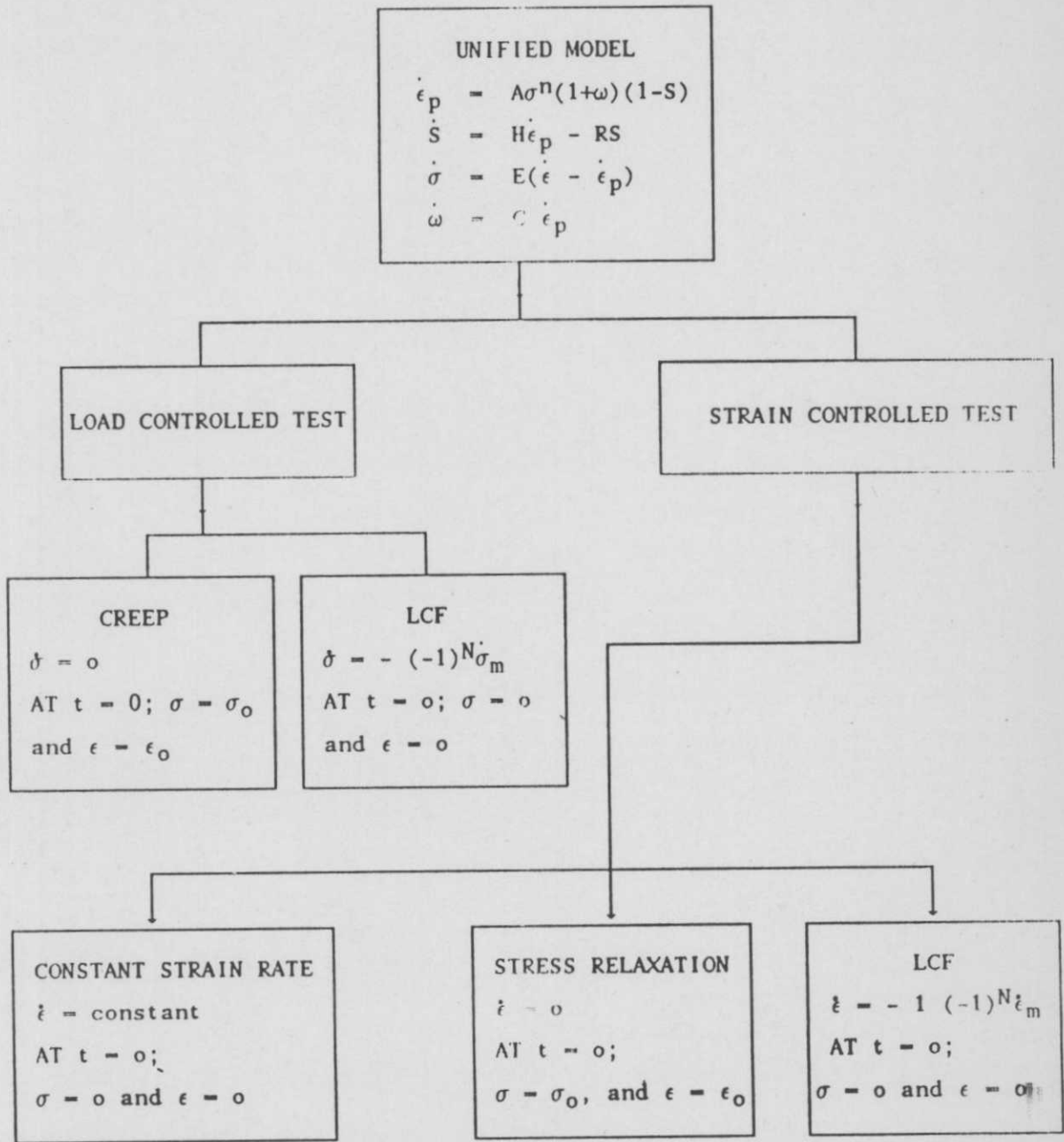


Fig 12 Unified constitutive model for uniaxial mechanical test. N is an integer. $\dot{\sigma}_m$ and $\dot{\epsilon}_m$ are mean stress and strain rates. See text for rest of the symbols.

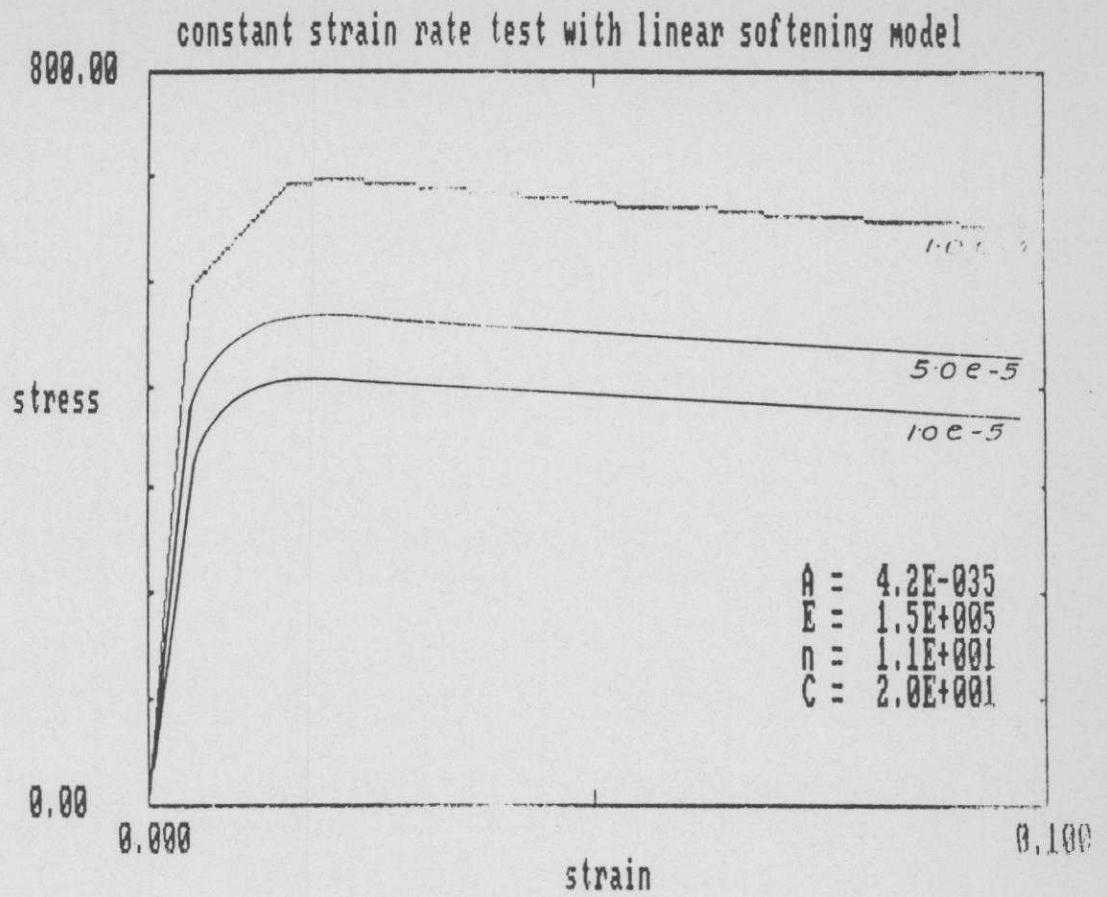


Fig 13

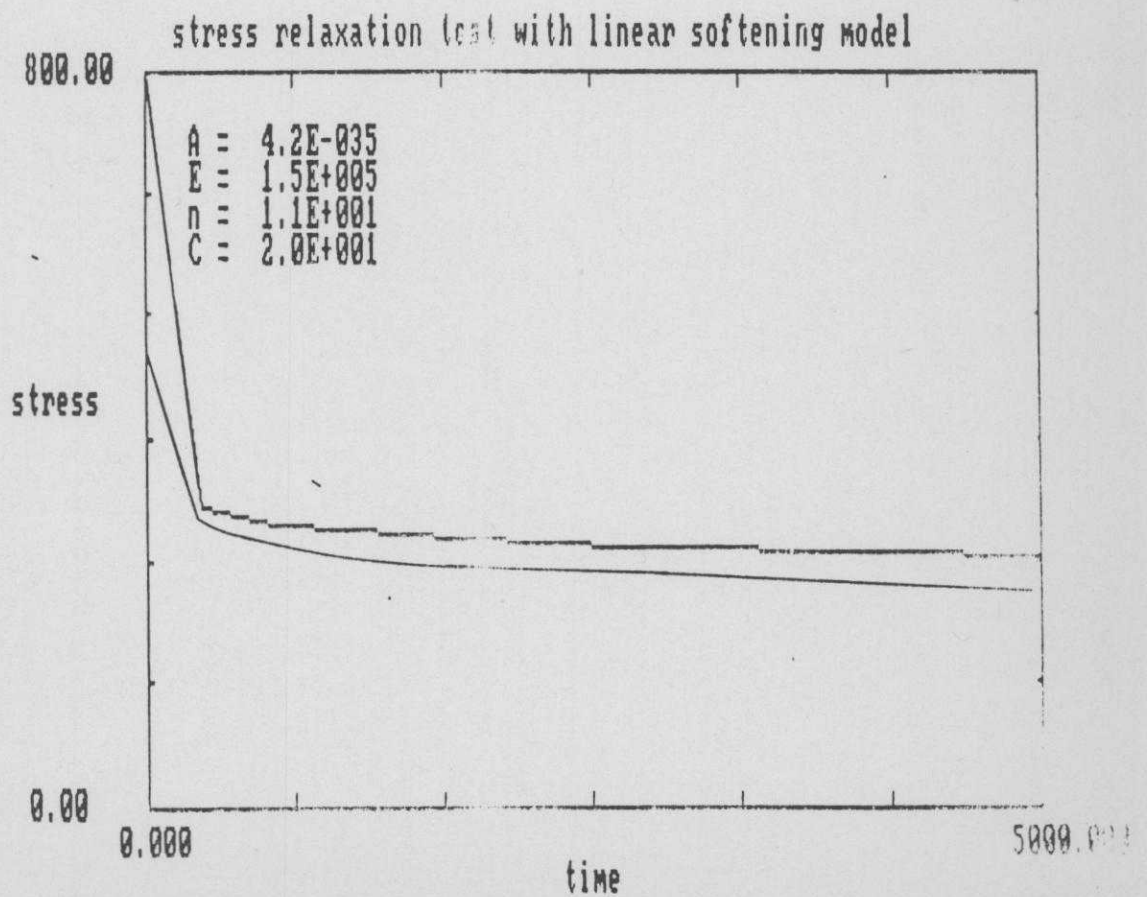


Fig 14

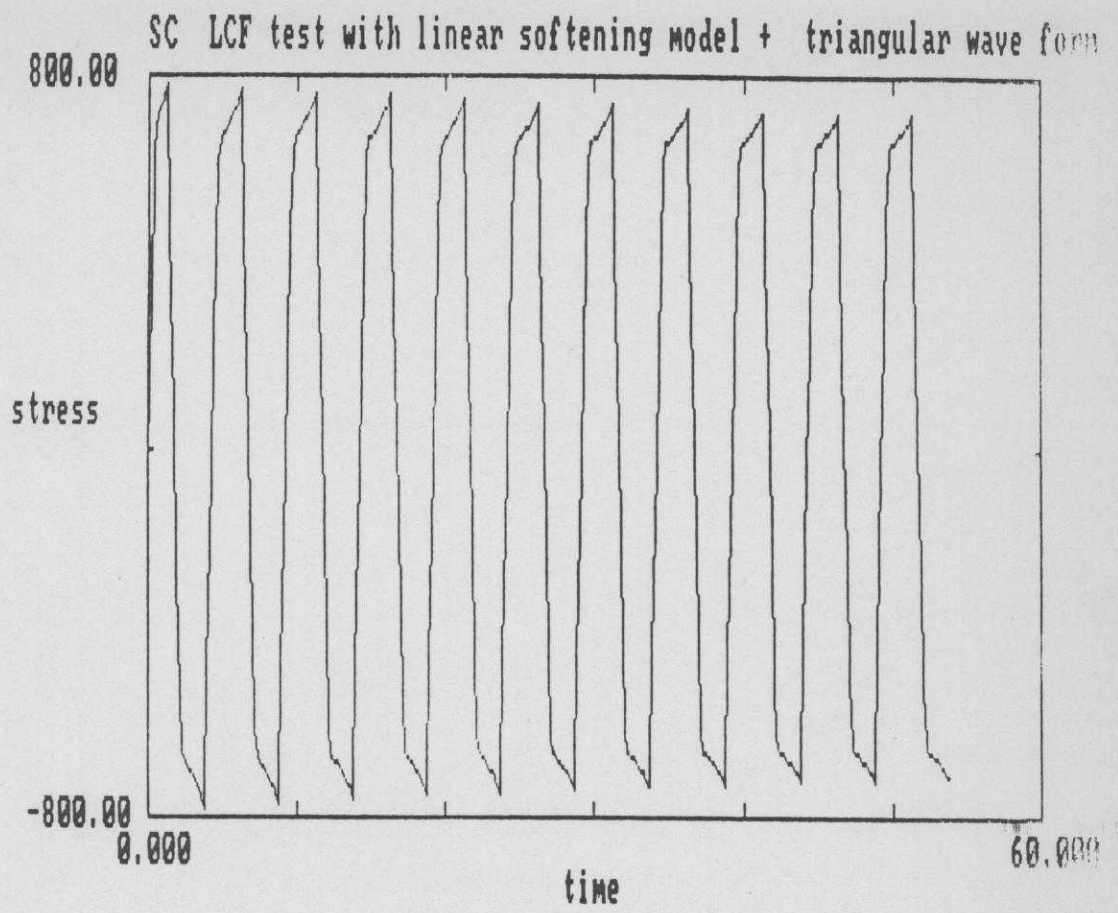


Fig 15a

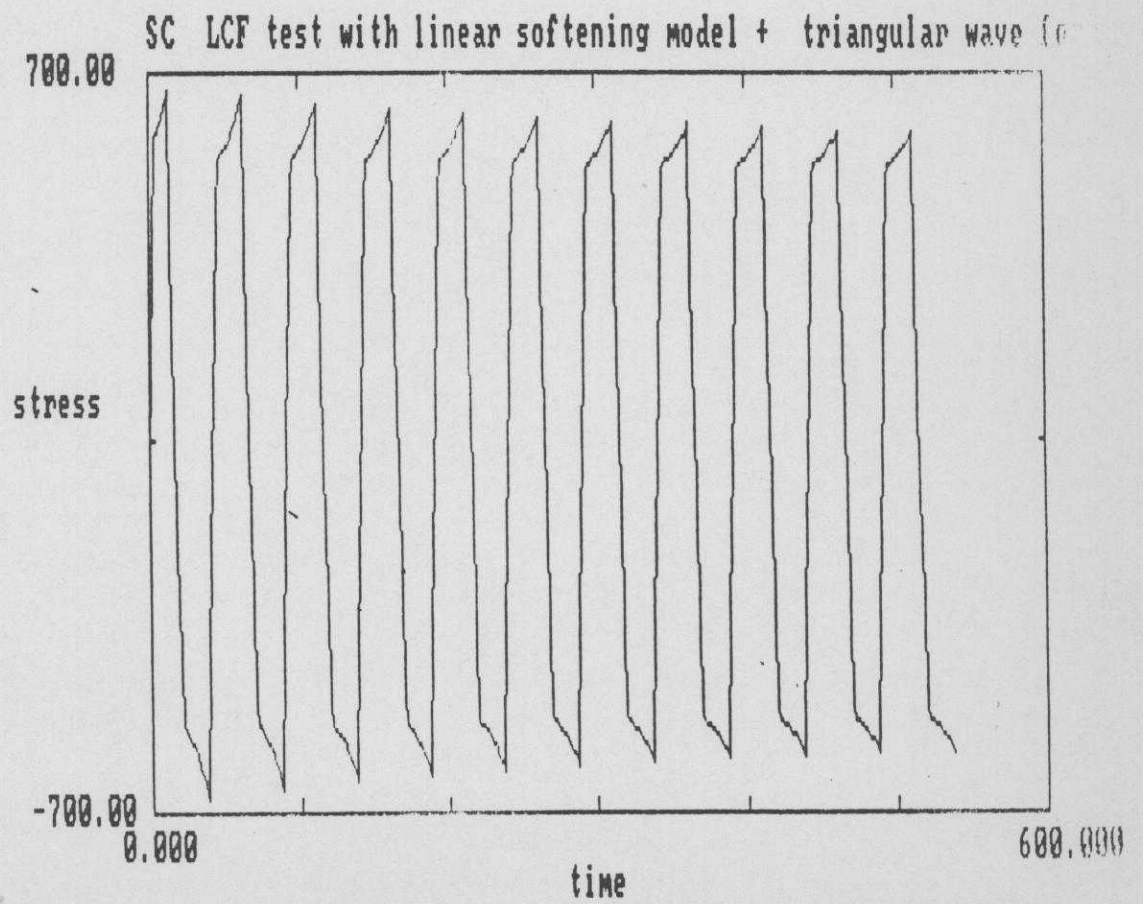


Fig 15b

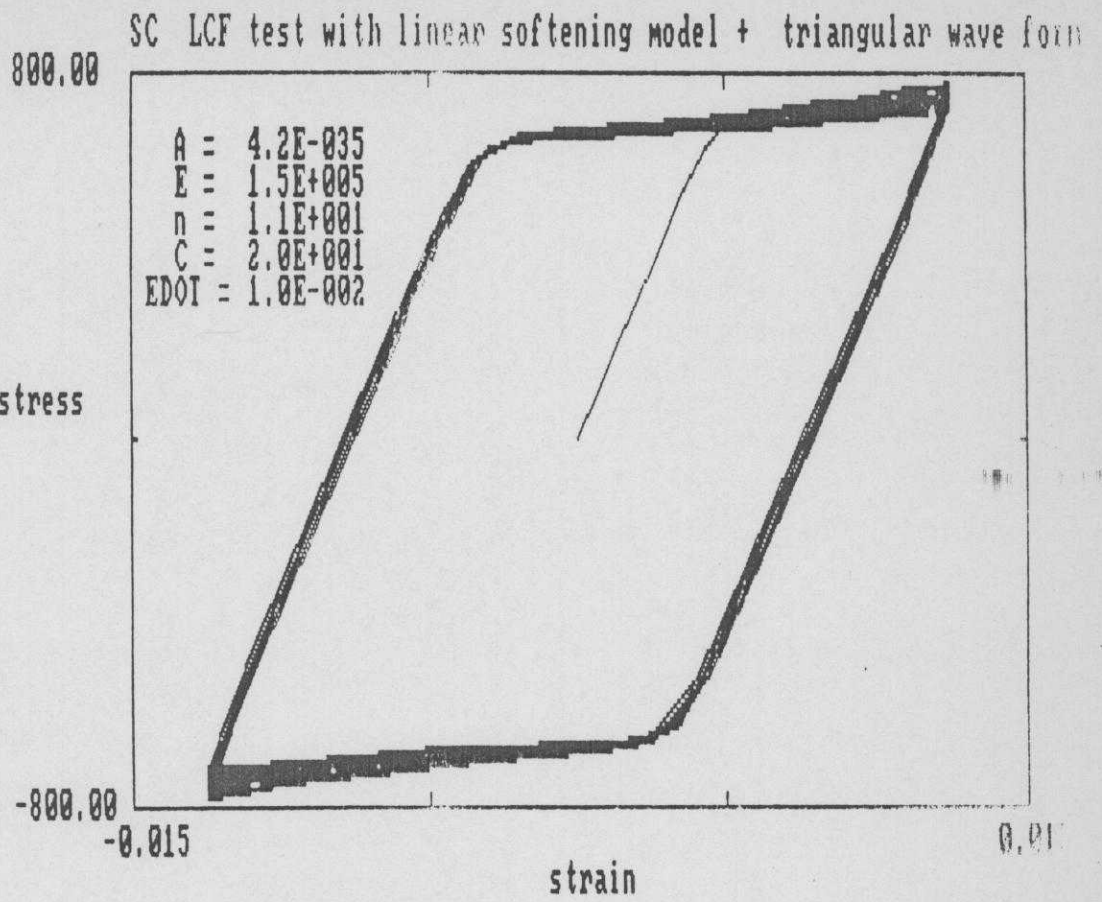


Fig 16a

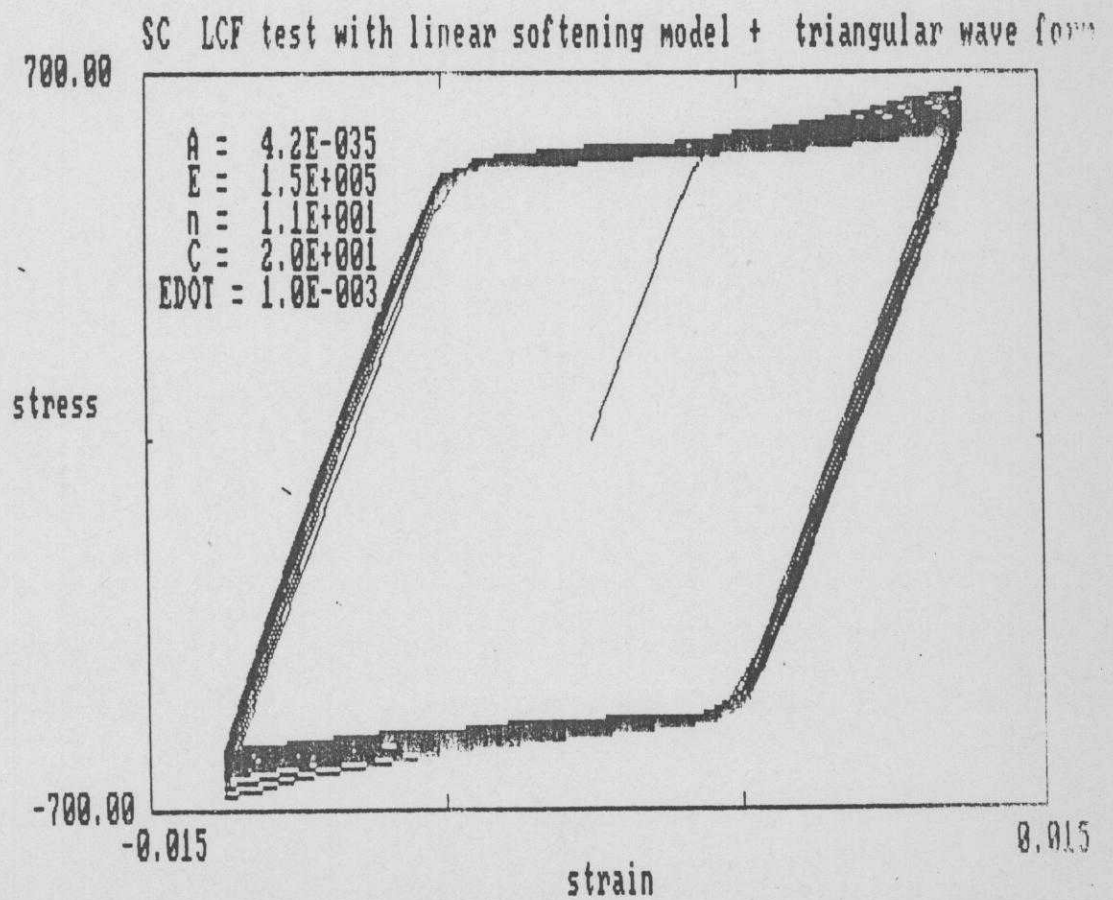


Fig 16b

SC LCF test with linear softening model + triangular wave form

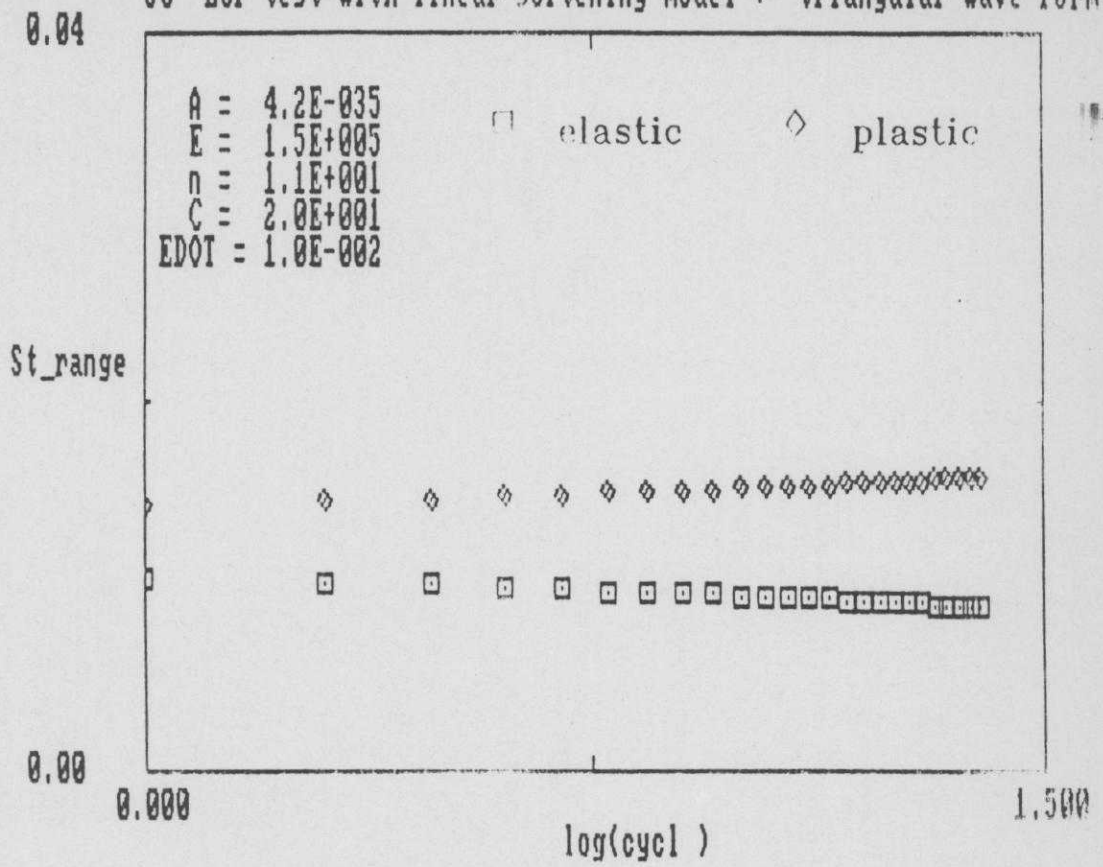


Fig 17a

SC LCF test with linear softening model + triangular wave form

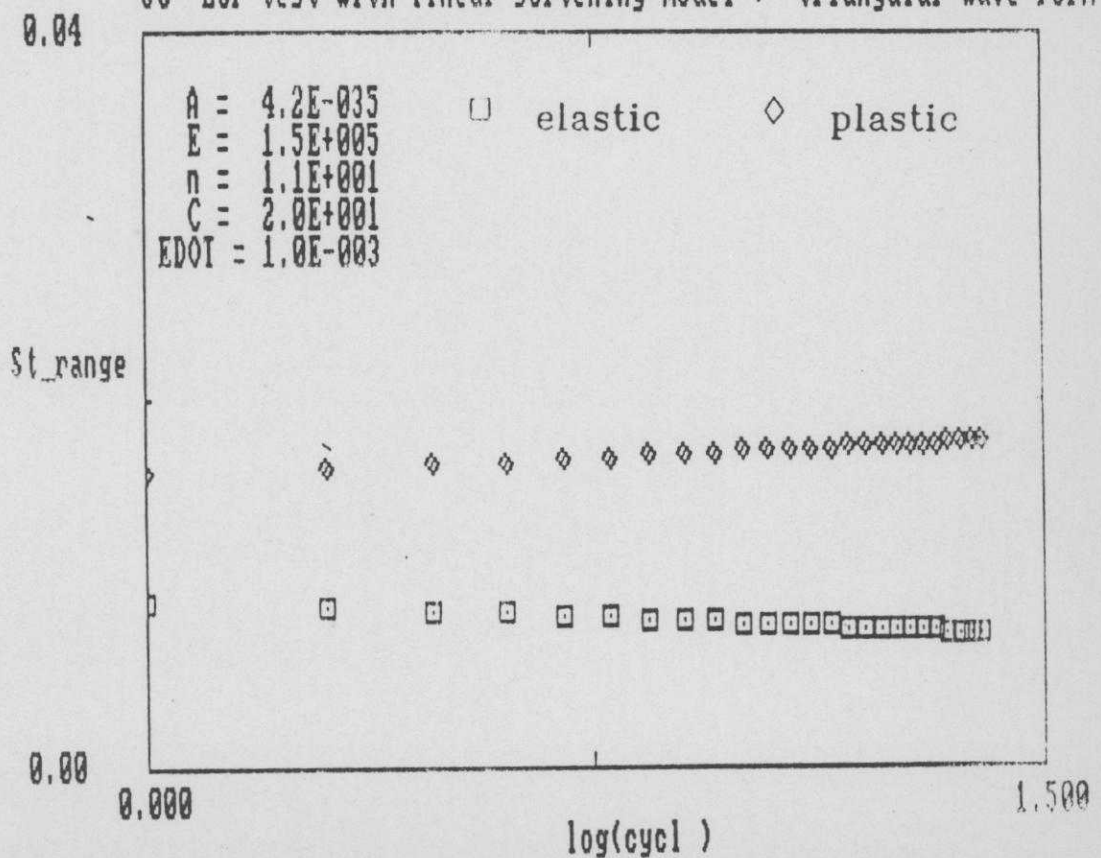


Fig 17b

LC LCF test with linear softening model + triangular wave form

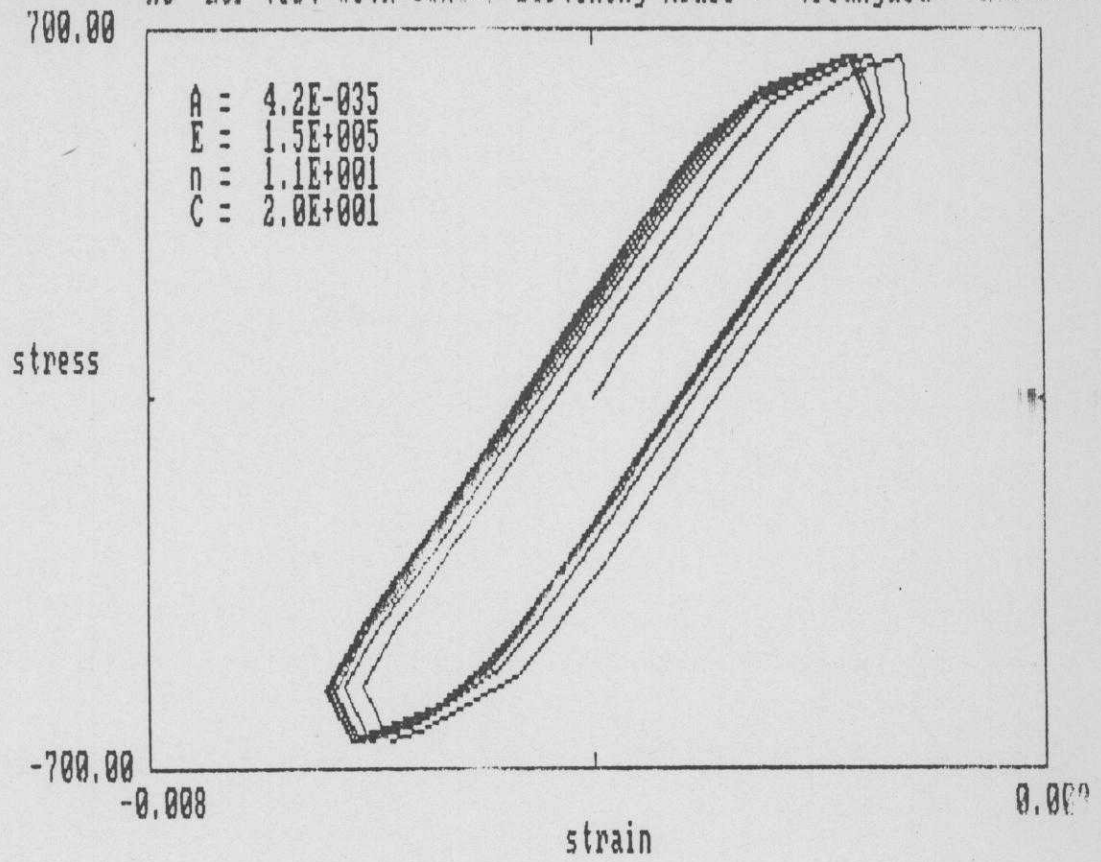


Fig 18a

LC LCF test with linear softening model + triangular wave form

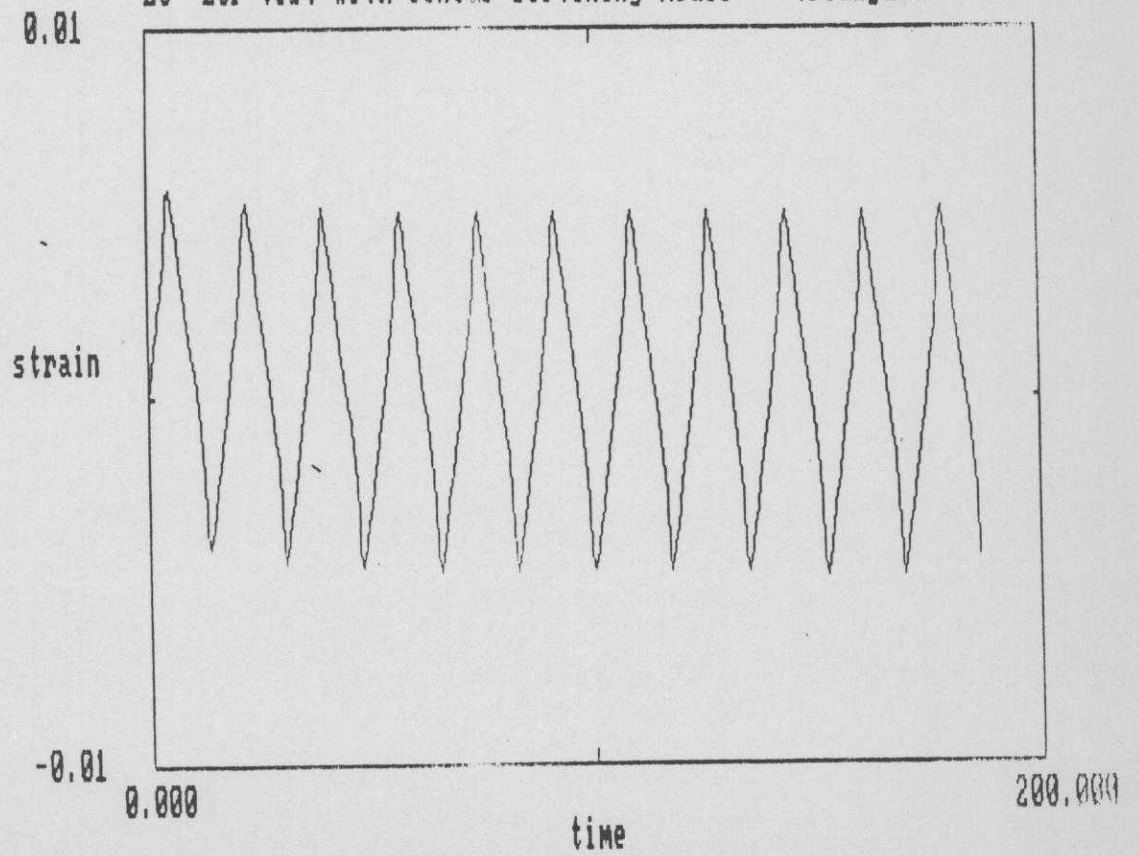


Fig 18b

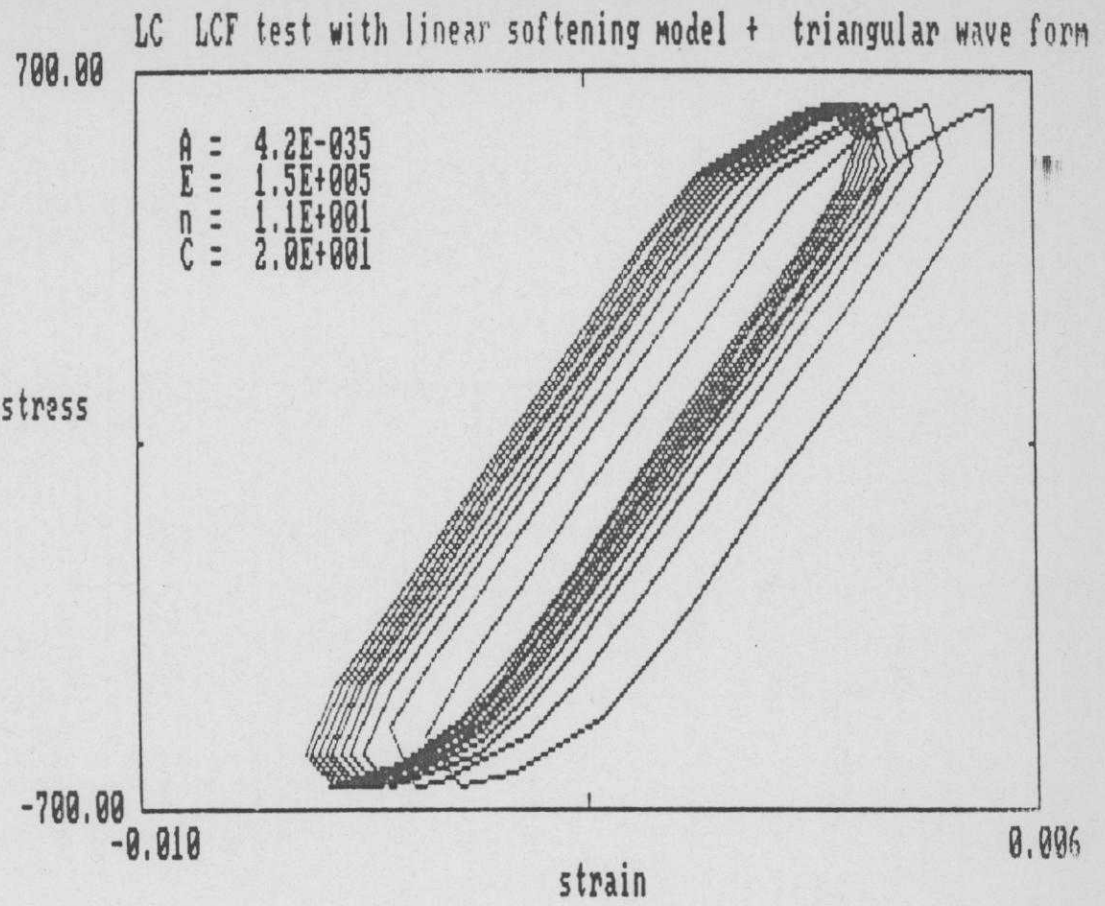


Fig 19a

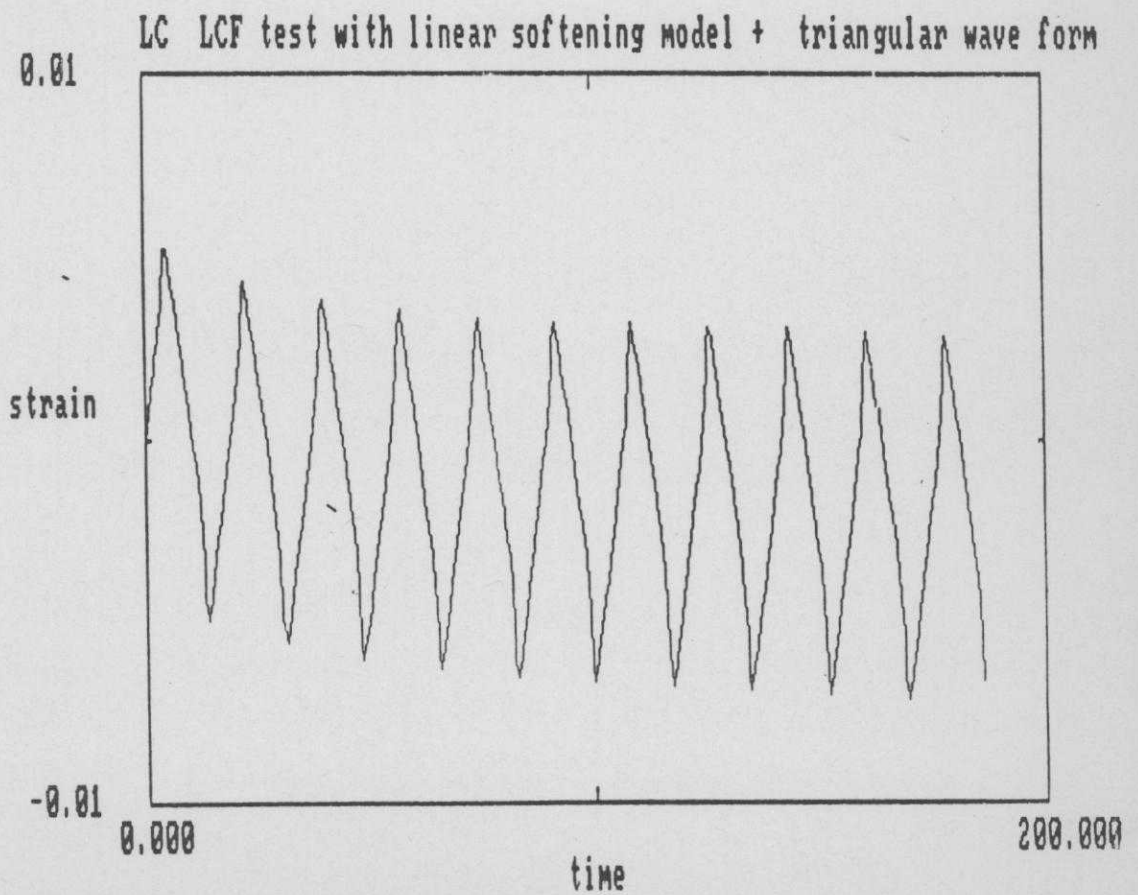


Fig 19b

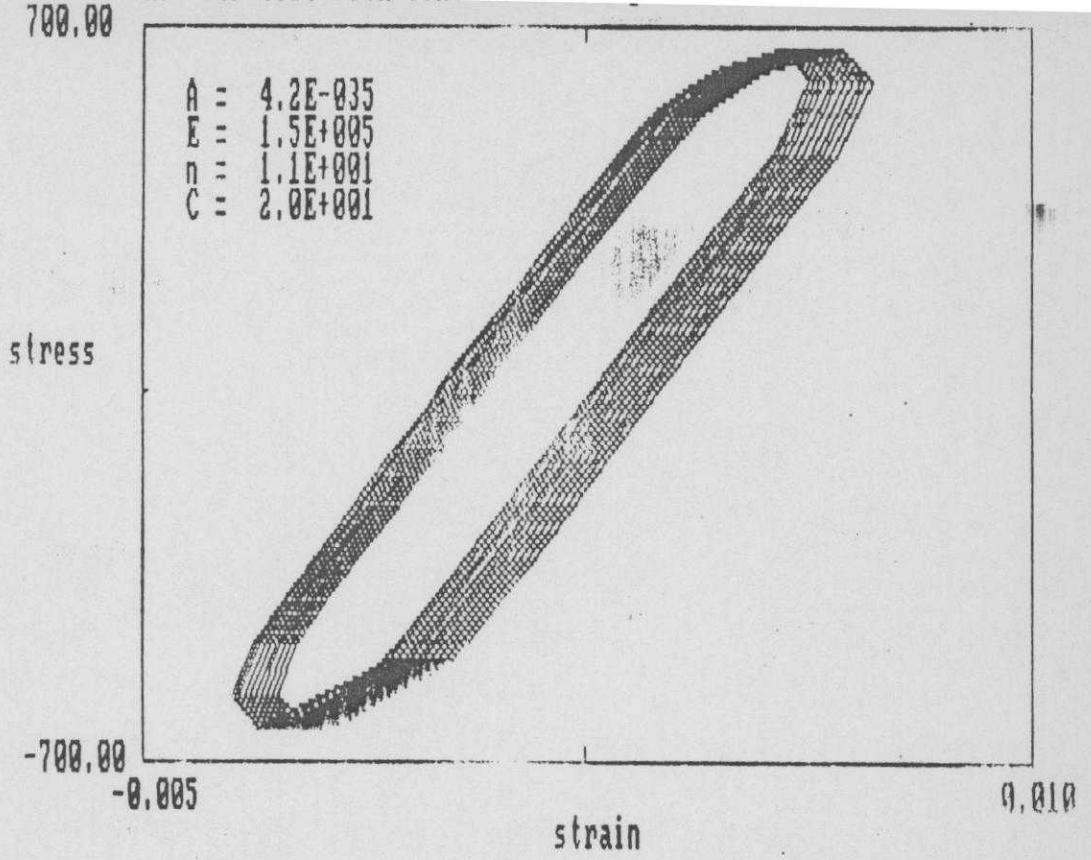


Fig 20a

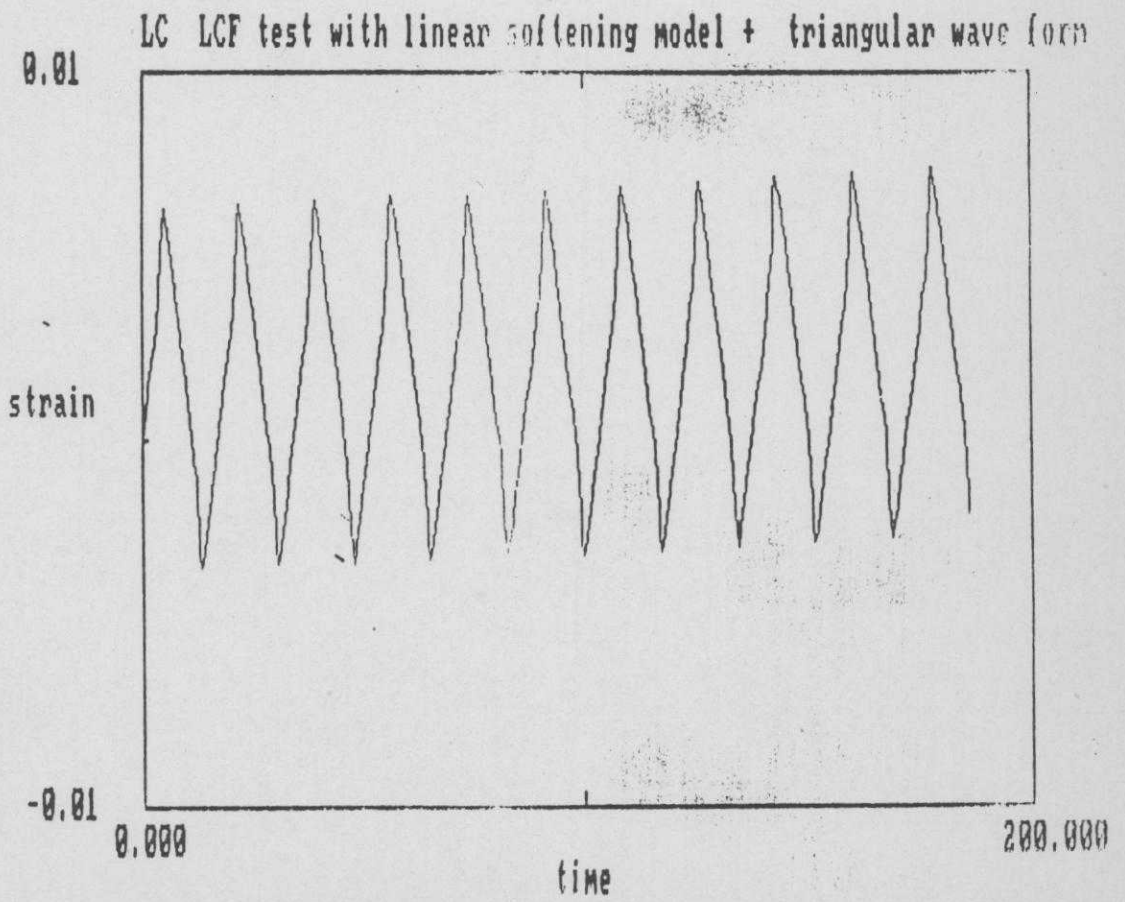


Fig 20b

LC LCF test with linear softening model + triangular wave form

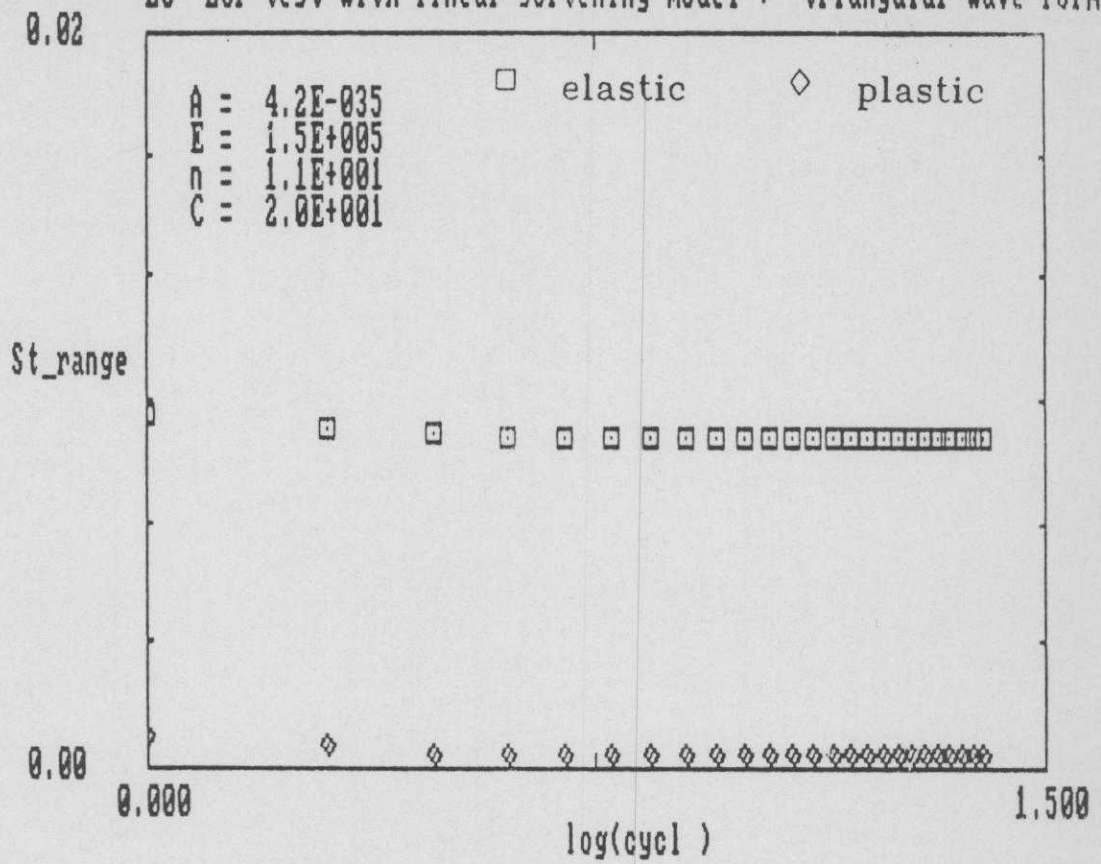


Fig 21a

LC LCF test with linear softening model + triangular wave form

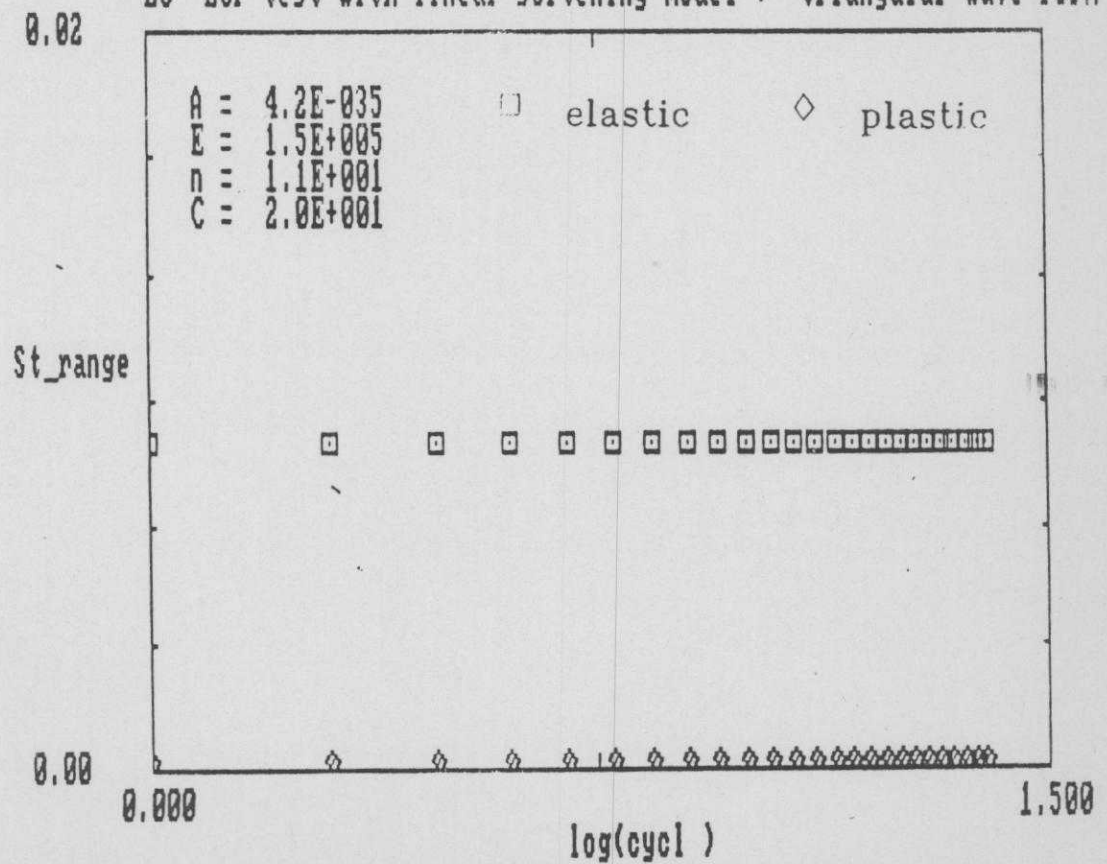


Fig 21b

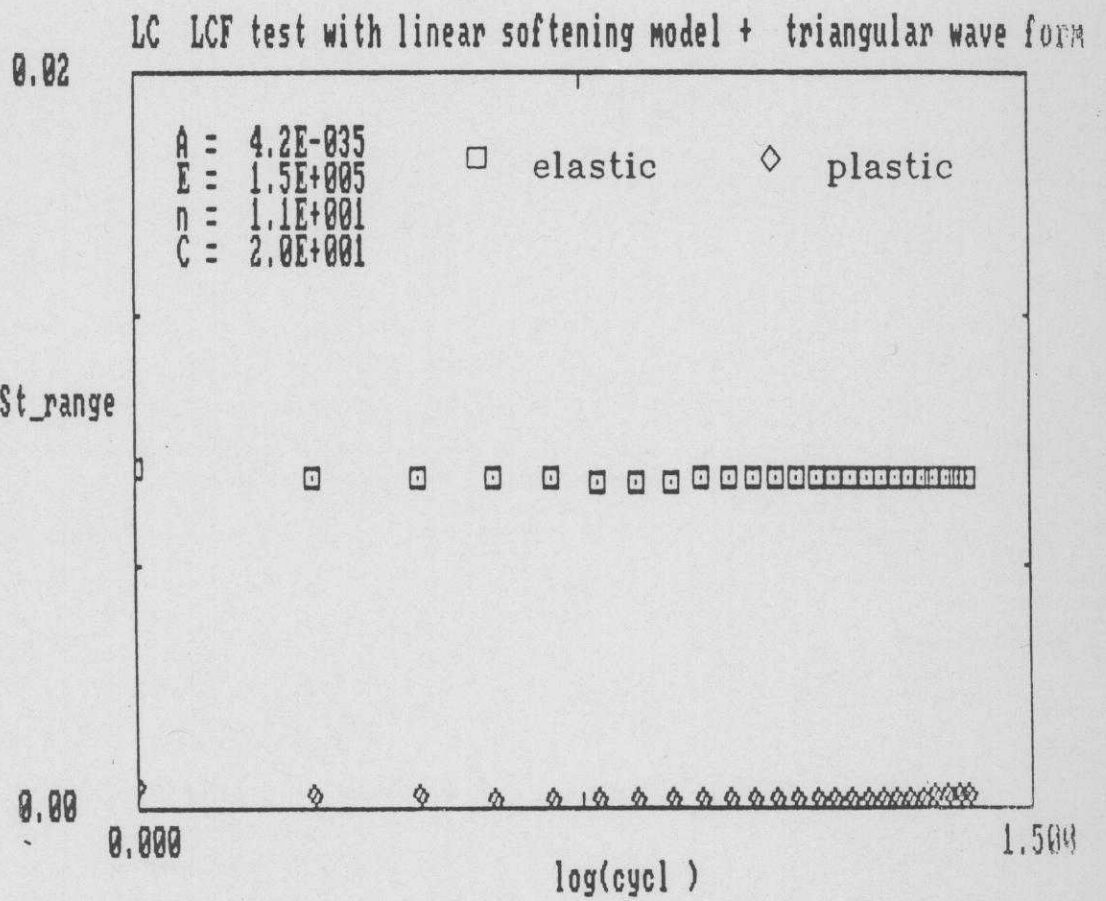


Fig 21c